

1 **Eddy covariance data reveal that a small freshwater reservoir emits a substantial**
2 **amount of carbon dioxide and methane**

3 **Alexandria G. Hounshell^{1, †}, Brenda M. D'Acunha², Adrienne Breef-Pilz¹, Mark S.**
4 **Johnson^{2,3}, R. Quinn Thomas^{1,4}, Cayelan C. Carey¹**

5 ¹ Department of Biological Sciences, Virginia Tech, Blacksburg, VA, USA, ² Department of
6 Earth, Ocean, and Atmospheric Sciences, University of British Columbia, Vancouver, BC,
7 Canada, ³ Institute for Resources, Environment and Sustainability, University of British
8 Columbia, Vancouver, BC, Canada, ⁴ Department of Forest Resources and Environmental
9 Conservation, Virginia Tech, Blacksburg, VA, USA

10 Corresponding author: Alexandria G. Hounshell (alexgh@vt.edu)

11 † Current affiliation: National Centers for Coastal Ocean Science, National Oceanographic and
12 Atmospheric Administration, Beaufort, NC, 28516 alexandria.hounshell@noaa.gov

13 **Key Points:**

- 14 • We measured high annual CO₂ (633-731 g C m⁻² yr⁻¹) and CH₄ (1.02-1.29 g C m⁻² yr⁻¹)
15 fluxes over 2 years from a small reservoir
- 16 • Fluxes were higher in the summer than winter, with statistically higher fluxes during
17 intermittent ice-on as compared to continuous ice-on
- 18 • Surface water temperature, thermocline depth, and dissolved organic matter
19 concentrations were correlated with reservoir fluxes

20 **Abstract**

21 Small freshwater reservoirs are ubiquitous and likely play an important role in global greenhouse
22 gas (GHG) budgets relative to their limited water surface area. However, constraining annual
23 GHG fluxes in small freshwater reservoirs is challenging given their footprint area and spatially
24 and temporally variable emissions. To quantify the GHG budget of a small (0.1 km²) reservoir,
25 we deployed an eddy covariance system in a small reservoir located in southwestern Virginia,
26 USA over two years to measure carbon dioxide (CO₂) and methane (CH₄) fluxes near-
27 continuously. Fluxes were coupled with *in situ* sensors measuring multiple environmental
28 parameters. Over both years, we found the reservoir to be a large source of CO₂ (633-731 g CO₂-
29 C m⁻² yr⁻¹) and CH₄ (1.02-1.29 g CH₄-C m⁻² yr⁻¹) to the atmosphere, with substantial sub-daily,
30 daily, weekly, and seasonal timescales of variability. For example, fluxes were substantially
31 greater during the summer thermally-stratified season as compared to the winter. In addition, we
32 observed significantly greater GHG fluxes during winter intermittent ice-on conditions as
33 compared to continuous ice-on conditions, suggesting GHG emissions from lakes and reservoirs
34 may increase with predicted decreases in winter ice-cover. Finally, we identified several key
35 environmental variables that may be driving reservoir GHG fluxes at multiple timescales,
36 including, surface water temperature and thermocline depth followed by fluorescent dissolved
37 organic matter. Overall, our novel year-round eddy covariance data from a small reservoir
38 indicate that these freshwater ecosystems likely contribute a substantial amount of CO₂ and CH₄
39 to global GHG budgets.

40

41 **Plain Language Summary**

42 Freshwater ecosystems release substantial amounts of greenhouse gases, especially carbon
43 dioxide and methane, to the atmosphere. Small waterbodies, such as lakes and reservoirs, are
44 common in the landscape and may release particularly high levels of greenhouse gases, though
45 their overall contribution remains unknown. The most common methods to date for estimating
46 greenhouse gas emissions from freshwaters typically involve only measuring concentrations
47 during the daytime on a handful of days throughout the year. Thus, there is a clear need for near-
48 continuous measurements of carbon dioxide and methane from small waterbodies throughout the
49 year on multiple timescales (hours to years). To do this, we measured near-continuous fluxes of

50 carbon dioxide and methane from a small reservoir using eddy covariance over two years. We
51 found this small reservoir to be a large source of both carbon dioxide and methane to the
52 atmosphere over two years and found high variability in fluxes measured at short (sub-daily) to
53 long (seasonal) timescales. Overall, this study demonstrates the importance of small reservoirs as
54 greenhouse gas sources to the atmosphere and emphasizes the need for additional measurements
55 to estimate their contribution to global greenhouse gas budgets.

56

57 **1 Introduction**

58 Freshwater ecosystems play a disproportionately large role in global greenhouse gas
59 (GHG) budgets relative to their total water surface area, often emitting more GHGs than are
60 taken up by terrestrial ecosystems (Bastviken et al. 2011; Cole et al. 2007; DelSontro et al. 2018;
61 Tranvik et al. 2009). Despite their importance, however, the contribution of inland waters
62 remains under-represented within global carbon (C) and GHG budgets (Butman et al. 2018;
63 Deemer and Holgerson, 2021; Deemer et al. 2016; DelSontro et al. 2018). To date, most studies
64 measuring GHG emissions from freshwater lakes and reservoirs are based on snapshot
65 measurements from short-term floating chamber deployments or grab samples of dissolved
66 GHGs, which are extrapolated to broad spatial and temporal scales to estimate annual whole-
67 ecosystem fluxes (Bastviken et al. 2015; Klaus et al. 2019; Wik et al. 2016). While these
68 approaches have provided useful insights into general patterns of GHG cycling in freshwater
69 ecosystems, they are inherently limited in capturing the high spatial and temporal variability in
70 freshwater GHG fluxes (A.K. Baldocchi et al. 2020; Butman et al. 2018; Klaus et al. 2019;
71 Rosentreter et al. 2021; Wik et al. 2016).

72 Among freshwater ecosystems, small ($<1 \text{ km}^2$) reservoirs may be particularly under-
73 represented in GHG budgets (Deemer and Holgerson, 2021; DelSontro et al. 2018; Rosentreter
74 et al. 2021). It is estimated that there are ~5.8 million lakes and reservoirs in the contiguous U.S.
75 (Winslow et al. 2014), of which approximately half (~2.6 million) are human-made reservoirs
76 (Smith et al. 2002). Small reservoirs ($<1 \text{ km}^2$) compose $>71\%$ of reservoirs in the United States
77 (National Inventory of Dams, USACE 2021), indicating that these ecosystems are extremely
78 common, with at least ~1.8 million small reservoirs in the conterminous U.S. However,

79 constraining annual GHG estimates in small freshwater reservoirs is challenging given their
80 small footprint area and heterogeneous GHG emissions (Loken et al. 2019; McClure et al. 2020;
81 Podgrajsek et al. 2015). Short-term measurements indicate the potential for these ecosystems to
82 exhibit high, but patchy fluxes (Deemer and Holgerson, 2021; DelSontro et al. 2018; McClure et
83 al. 2018, 2020; Rosentreter et al. 2021), but to the best of our knowledge their annual emissions
84 remain largely unknown.

85 Eddy covariance (EC) systems are increasingly being deployed on lakes and reservoirs to
86 constrain sub-daily GHG fluxes over large spatial footprints, enabling the quantification of
87 whole-ecosystem GHG fluxes at multiple temporal scales (e.g., A.K. Baldocchi et al. 2020;
88 Golub et al. 2021; Eugster et al. 2011; Vesala et al. 2011; Waldo et al. 2021). EC systems are
89 used to determine the net exchange of carbon dioxide (CO₂), methane (CH₄), and/or other gases
90 at sub-hourly time scales via micrometeorology and *in situ* atmospheric trace gas concentrations
91 measured using infrared gas analyzers (A.K. Baldocchi et al. 2020; Golub et al. 2021; Vesala et
92 al. 2011). By collecting near-continuous, high frequency data (typically measured at 10-20 Hz
93 and reported as 30-minute means), EC systems allow GHG fluxes to be estimated at sub-daily to
94 annual timescales, improving our understanding of GHG flux temporal variability beyond
95 traditional discrete measurements (Golub et al. 2021; Reed et al. 2018; Vesala et al. 2011).
96 Additionally, EC systems often capture a larger spatial footprint compared to traditional discrete
97 measurements, as measured fluxes represent the average flux from the atmospherically-mixed
98 area upwind of the deployed EC system (Golub et al. 2021, Waldo et al. 2021). Thus, EC
99 systems can greatly increase the temporal and spatial resolution of measured fluxes in lakes and
100 reservoirs, with the caveat that important considerations and data filtering are needed for EC
101 systems in small waterbodies (Scholz et al. 2021). Specifically, a waterbody's small surface area
102 increases the likelihood of surrounding terrestrial vegetation impacting EC measurements of
103 aquatic fluxes and decreases the area available for a well-mixed, turbulent footprint (Esters et al.
104 2020; Scholz et al. 2021; Vesala et al. 2011).

105 While the majority of reported freshwater EC studies have been conducted on short
106 timescales (days to months; e.g., Erkkilä et al. 2018; Gorsky et al. 2021; Jammot et al. 2015;
107 Podgrajsek et al. 2014, 2015; Vesala et al. 2006, 2011), longer-term studies measuring CO₂ or
108 CH₄ fluxes in lakes and reservoirs on annual timescales are now becoming more common (e.g.,
109 A.K. Baldocchi et al. 2020; Golub et al. 2021; Jammot et al. 2017; Liu et al. 2016; Reed et al.

110 2018; Shao et al. 2015; Scholz et al. 2021; Taoka et al. 2020; Waldo et al. 2021). An annual
111 study conducted in Lake Erie, USA found this highly-eutrophic system was a small sink of CO₂
112 during the summer productive season yet ultimately a CO₂ source on annual timescales (Shao et
113 al. 2015). Other studies have highlighted the importance of short (hourly to daily), episodic
114 events on annual CO₂ budgets, including the disproportionate effect of storms on annual CO₂
115 emissions from a large subtropical reservoir (Liu et al. 2016), fall mixing in a large (40 km²)
116 temperate lake (Reed et al. 2018), and pulses of CH₄ following ice-off in a north temperate lake
117 (Gorsky et al. 2021). Annual studies have also revealed low and relatively consistent CO₂ fluxes
118 during the winter ice-covered period (A.K. Baldocchi et al. 2020; Reed et al. 2018). In addition
119 to noted diel, seasonal, and episodic variability in CO₂ fluxes, two annual studies recently found
120 the sub-monthly timescale to be an important timescale of variability, though the mechanism for
121 this variability remains unknown (A.K. Baldocchi et al. 2020; Golub et al. 2021). Despite the
122 increase in studies using EC systems to measure CO₂ and CH₄ fluxes from freshwaters, few
123 studies to date have captured both CO₂ and CH₄ fluxes on the annual scale, especially during
124 winter.

125 Measuring annual-scale CO₂ and CH₄ fluxes is particularly important as GHG fluxes are
126 likely rapidly changing due to altered climate (Bartosiewicz et al. 2019; Beaulieu et al. 2019),
127 motivating several potential hypotheses for how different environmental drivers may alter fluxes.
128 Multiple drivers sensitive to climate change likely affect GHG fluxes, though annual-scale
129 studies to test the effects of these drivers on fluxes across multiple timescales are lacking. For
130 example, increasing surface temperatures and changes in precipitation and nutrient loading are
131 changing phytoplankton productivity and allochthonous C inputs to lakes and reservoirs (Fowler
132 et al. 2020; Hanson et al. 2015; Tranvik et al. 2009). Changes in freshwater primary production
133 and nutrient inputs to freshwater systems have been directly linked to changes in CO₂ (DelSontro
134 et al. 2018), as well as CH₄ emissions (Deemer and Holgerson, 2021; DelSontro et al. 2018;
135 McClure et al. 2020). Finally, increasing air temperatures are leading to warmer winters and
136 more intermittent and partial ice cover (Imrit and Sharma, 2021; Sharma et al. 2021; Woolway et
137 al. 2020), highlighting the need to understand the role of ice in constraining GHG fluxes. All
138 these examples emphasize the importance of measuring near-continuous GHG fluxes on the
139 annual scale along with key potential environmental drivers, such as precipitation and freshwater
140 inflows, air and water temperature, chlorophyll-*a*, dissolved organic matter, and ice-on/ice-off as

141 potential GHG drivers, as it is likely that some drivers may have a greater effect at certain
142 timescales than others.

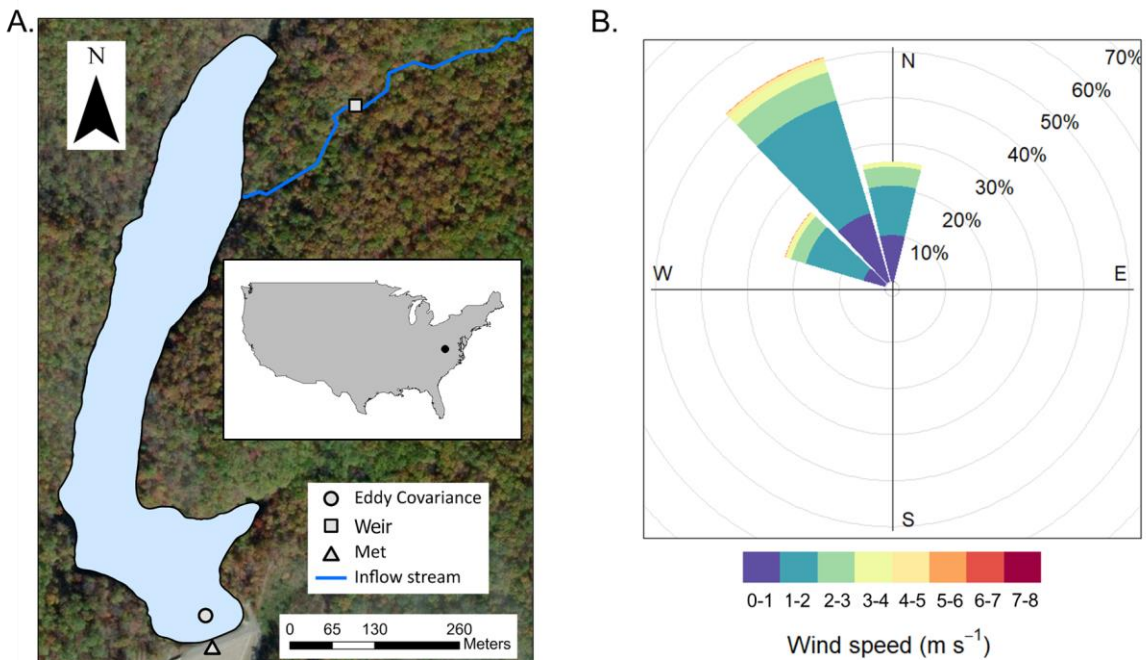
143 Altogether, there is a clear need to measure annual-scale CH₄ and CO₂ fluxes from small
144 freshwater ecosystems, especially small reservoirs. To the best of our knowledge, only one
145 freshwater study has measured both CH₄ and CO₂ fluxes on an annual timescale (Jammet et al.
146 2017), while Waldo et al. (2021) measured only CH₄ fluxes at the annual scale. Waldo et al.
147 (2021) used EC to measure annual CH₄ fluxes from a large (2.4 km²), highly-eutrophic temperate
148 reservoir, measuring emissions up to 71.4 g CH₄ m⁻² yr⁻¹, which is in the top quarter of those
149 reported from lakes and reservoirs to date. In an Arctic lake, Jammet et al. (2017) used EC to
150 measure low GHG fluxes during ice cover, followed by large CH₄ and CO₂ fluxes during spring-
151 thaw, and increasing ebullitive CH₄ fluxes during the ice-free season concurrent with high rates
152 of CO₂ uptake due to photosynthesis. Aggregated across the full year, this Arctic lake was a net
153 source of both CH₄ and CO₂ to the atmosphere (Jammet et al. 2017). Across the literature, most
154 EC studies have focused on naturally-formed lakes, and all EC reservoir studies of which we are
155 aware (Eugster et al. 2011; Golub et al. 2021; Liu et al., 2016; Waldo et al. 2021) were
156 conducted in large (>2.4 km²) reservoirs.

157 To better understand the GHG budgets of small reservoirs and identify key environmental
158 drivers, we deployed an EC system in a small (0.1 km²) freshwater reservoir located in
159 southwestern Virginia, USA for two years to measure CO₂ and CH₄ fluxes near-continuously.
160 Flux measurements were coupled with *in situ* sensors measuring multiple environmental
161 parameters, including surface water temperature, dissolved oxygen, chlorophyll-*a*, and
162 fluorescent dissolved organic matter. We used the measured GHG fluxes to answer the
163 questions: 1) What is the annual phenology of CO₂ and CH₄ fluxes in a small, eutrophic
164 reservoir, including during the critical winter period?; and 2) Which environmental variables best
165 explain CO₂ and CH₄ variability at daily to monthly timescales?

166 **2 Materials and Methods**

167 2.1 Site description

168 Falling Creek Reservoir (FCR) is a small, eutrophic reservoir located in Vinton, Virginia,
169 USA (Fig. 1; 37.30°N, 79.84°W; Howard et al. 2021). The reservoir and surrounding forested
170 watershed are owned and operated by the Western Virginia Water Authority (WVWA) as a
171 primary drinking water source (Gerling et al. 2016). FCR has a surface area of 0.119 km² and
172 maximum depth of 9.3 m (McClure et al. 2018). The reservoir is dimictic and thermally stratified
173 from April to October (McClure et al. 2018). During the study period, water was not extracted
174 for drinking water treatment and remained at a constant full-pond level.



175
176 **Figure 1.** A. Map of Falling Creek Reservoir (FCR) located in Vinton, Virginia, USA (map
177 inset) showing location of the eddy covariance system, the weir located on the primary
178 freshwater inflow, and the meteorological station located on the dam. B. Wind rose showing the
179 dominant wind direction and wind speed (m s^{-1}) of greenhouse gas fluxes retained for analysis.
180 The cumulative footprint distribution for the whole study period is shown in the supplementary
181 information (Fig. S1).

182 2.2 Data collection and overview

183 We used an EC system to measure CO₂ and CH₄ fluxes between the water surface and the
184 atmosphere from 1 May 2020 to 30 April 2022 (details below; Carey et al. 2022a). To
185 complement the EC measured fluxes, we also calculated CO₂ and CH₄ diffusive gas fluxes using
186 dissolved CO₂ and CH₄ discrete grab samples collected during daylight hours (between ~0800 to
187 1300) weekly to monthly from the water's surface at the deepest site of the reservoir, located near
188 the dam, throughout the 2-year study period (details below; Carey et al. 2022b).

189 In addition to the EC and diffusive fluxes, we also collected meteorological and
190 environmental data. Briefly, a Campbell Scientific (Logan, Utah, USA) research-grade
191 meteorological station measured air temperature; relative humidity; air pressure; wind speed and
192 direction; upwelling and downwelling shortwave and longwave radiation; total rainfall;
193 photosynthetically-active radiation (PAR); and albedo every minute at the reservoir dam (sensor
194 information provided by Carey et al. 2022c). At the reservoir's deepest site, we collected 10-
195 minute water temperature measurements every 1 m from the surface (0.1 m) to just above the
196 sediments (9 m) using a thermistor string. Thermistor data were used to calculate the difference
197 in temperature between 0.1 m and 9.0 m (Diff. Temp) and daily buoyancy frequency (N^2), two
198 metrics of thermal stratification, as well as thermocline depth throughout the study period (May
199 2020 to April 2022) using the LakeAnalyzer package in R (Winslow et al. 2016a). Fall turnover
200 was defined as the first day in autumn when the temperature at 1 m was $<1^\circ\text{C}$ of the temperature
201 measured at 8 m (1 November 2020 and 3 November 2021; McClure et al. 2018). Spring mixing
202 was harder to identify due to intermittent ice-on in 2021, but we defined spring mixing as the
203 first day in spring after complete ice-off when the temperature at 1 m was $<1^\circ\text{C}$ of the
204 temperature measured at 8 m (26 February 2021 and 10 February 2022). Ice cover was
205 determined by the presence of inverse stratification coupled with higher albedo and verified by
206 visual observation, described by Carey and Breef-Pilz (2022).

207 Water column temperature data complemented 10-minute measurements of dissolved
208 oxygen (DO) percent saturation, chlorophyll-*a* (Chl-*a*, $\mu\text{g L}^{-1}$), and fluorescent dissolved organic
209 matter (fDOM, relative fluorescent units, RFU) measured using an EXO2 sonde (YSI, Yellow
210 Springs, Ohio, USA) deployed at 1.6 m (Carey et al. 2022d). The EXO2 sonde was removed

211 from the reservoir on 2 December 2020 for annual sensor maintenance and re-deployed on 27
212 December 2020. Finally, we measured stream inflow every 15 minutes on the primary inflowing
213 stream to the reservoir via a gaged v-notch weir fitted with a Campbell Scientific CS451 pressure
214 transducer (Campbell Scientific, Logan, Utah, USA), which was used to calculate the 15-minute
215 flow rate following (Carey et al. 2022e). The weir was breached on 20 July 2020 and repaired on
216 24 August 2020, resulting in no flow data during this interval.

217 2.3 Eddy covariance flux measurements

218 An EC system was deployed above the water surface over the deepest portion of the
219 reservoir from 1 May 2020 to 30 April 2022. The EC instrumentation was installed on a
220 permanent metal platform that extends ~45 m from the dam and 2.9 m over the reservoir's
221 surface. As noted above, the reservoir was maintained at full pond, resulting in a consistent
222 height of the EC system over the water's surface during the study period. The EC system
223 included an ultrasonic anemometer to measure 3D wind speed and direction (CSAT3, Campbell
224 Scientific), an open-path infrared gas analyzer for measuring CH₄ concentration (LI-7700, LiCor
225 Biosciences, Lincoln, Nebraska, USA), and an enclosed-path infrared gas analyzer for measuring
226 CO₂ and water vapor concentrations (LI-7200, LiCor Biosciences), all recorded at 10 Hz by a
227 data logger (LI-7550, LiCor Biosciences). On 10 August 2020, the data logger was removed for
228 maintenance and re-deployed on 2 September 2020. Additionally, a thermocouple on the CO₂
229 sensor (LI-7200) was inoperable starting on 5 April 2021 and was repaired on 26 April 2021.

230 The raw 10-Hz data were first processed into 30-minute fluxes using the EddyPro v.7.0.6
231 software (LiCor Biosciences 2019). Fluxes were calculated following standard methods in
232 EddyPro v.7.0.6 (LiCor Biosciences 2019), which included spike detection and removal (Vickers
233 and Mahrt, 1997), a double rotation for tilt correction (Wilczak et al. 2001), linear detrending
234 (Gash and Culf, 1996), time lag compensation, and spectral corrections for high and low-pass
235 filtering effects following Moncrieff et al. (2004) and Moncrieff et al. (1997), respectively. In
236 addition, CH₄ molar density was corrected to account for air density fluctuations and
237 spectroscopic effects of temperature, pressure and water vapor following Webb et al. (1980).

238 This correction was not needed for CO₂, as fluxes were estimated using mixing ratios instead of
239 densities (Burba et al. 2012).

240 Following initial flux calculations and processing in EddyPro, we conducted additional
241 data processing following standard best practices, including: 1) removing wind directions which
242 originated outside of the reservoir (80-250°; Fig. 1); 2) removing extreme flux values (CO₂
243 fluxes $\geq |100| \mu\text{mol C m}^{-2} \text{ s}^{-1}$; CH₄ fluxes $\geq |0.25| \mu\text{mol C m}^{-2} \text{ s}^{-1}$); 3) removing CH₄ fluxes when
244 signal strength <20%; 4) removing CO₂ and CH₄ fluxes when they did not pass the test for
245 stationarity or developed turbulent conditions (QC, quality control level 2 per Mauder and
246 Foken, 2006), in addition to when the latent heat (LE) or sensible heat flux (H) had QC level <2;
247 5) removing open-path CH₄ fluxes during periods of rainfall, which was determined based on the
248 rain gauge deployed at the dam; 6) removing additional periods of low turbulence friction
249 velocity (u^*), as described below; and 7) removing data that corresponded to flux footprints that
250 extended significantly beyond the reservoir.

251 Finally, we used REddyProc (Wutzler et al. 2021) to determine the u^* threshold for
252 sufficiently turbulent conditions and removed any fluxes where u^* was $< 0.075 \text{ m s}^{-1}$. To account
253 for the uncertainty of estimating the u^* threshold, we used bootstrapping to estimate the
254 distribution of u^* thresholds, and obtained the 5th, 50th and 95th percentiles of this distribution
255 (0.070, 0.075, and 0.163 m s^{-1} , respectively; Wutzler et al., 2018).

256 Flux footprints were modeled for each half-hour using a simple, two-dimensional
257 parameterization developed by Kljun et al. (2015) (Fig. S1). This model builds on the
258 Lagrangian stochastic particle dispersion model (Kljun et al. 2002), and provides information on
259 the extent, width, and shape of the footprint. All the variables needed for the model were
260 obtained directly from the dataset described above or calculated following Kljun et al. (2015).
261 Fluxes were excluded when the along-wind distance providing 90% cumulative contribution to
262 turbulent fluxes was outside the reservoir, based on the footprint analysis. We chose to use this
263 filtering threshold given the challenges of modeling footprints in small reservoirs; consequently,
264 our fluxes are likely conservative. All post-processing analyses were conducted using R

265 statistical software (v.4.0.3). Code for post-processing and all EC data can be found in the
266 Environmental Data Initiative (EDI) repository (Carey et al. 2022a).

267 2.4 Diffusive flux measurements

268 We estimated discrete diffusive fluxes from FCR using dissolved CO₂ and CH₄ samples
269 (Carey et al. 2022b) collected at the surface of the reservoir to compare with EC fluxes. Surface
270 water samples were collected at 0.1 m depth using a 4-L Van Dorn sampler (Wildlife Supply
271 Co., Yulee, Florida, USA) adjacent to the EC sensors (Fig. 1). Replicate (n=2) water samples
272 were collected via a Van Dorn sampler into 20-mL serum vials without headspace, immediately
273 capped, and then stored on ice until analysis within 24 hours. Samples were analyzed following
274 Carey et al. (2022b) on a Shimadzu Nexis GC-2030 Gas Chromatograph (Kyoto, Japan) with a
275 Flame Ionization Detector (GC-FID) and Thermal Conductivity Detector (TCD).

276 The measured surface samples were used to calculate CO₂ and CH₄ diffusive fluxes from
277 the surface of FCR into the atmosphere on each day of sample collection following the equation:

$$278 \text{ Flux} = k * (C_{\text{eq}} - C_{\text{air}}) \quad \text{Eq. 1}$$

279 where k is the gas transfer velocity (m d⁻¹) corrected for temperature and gas species (CO₂ or
280 CH₄, respectively), C_{eq} is the concentration of CO₂ or CH₄ at the reservoir surface (0.1 m), and
281 C_{air} is the atmospheric concentration of CO₂ or CH₄ measured by the EC system (Cole and
282 Caraco, 1998). The k value was calculated for each time point using multiple methods included
283 in the LakeMetabolizer package in R (Cole and Caraco, 1998; Crusius and Wannikof 2003;
284 Heiskanen et al. 2014; MacIntyre et al. 2010; Read et al. 2012; Soloviev et al. 2007; Vachon and
285 Prairie, 2013; Winslow et al. 2016b, 2016c). Both surface GHG replicates (n=2) calculated with
286 each k method, were used to calculate fluxes; the resultant mean and standard deviation are
287 reported.

288 2.5 Statistical analyses

289 To assess the phenology of fluxes (CO₂ and CH₄), we analyzed the mean and standard
290 deviation (±1 S.D.) of measured EC fluxes at half-hourly, daily, weekly, and monthly time scales
291 through the study period. For both EC and discrete diffusive fluxes, negative fluxes correspond

292 to fluxes into the reservoir (i.e., uptake) while positive fluxes are out of the reservoir (i.e., release
293 to the atmosphere).

294 To assess diel variation in GHG fluxes, we compared median measured EC fluxes during
295 the day (1100 to 1300) and night (2300 to 0100) throughout the year. As data were not normally
296 distributed, we used paired Wilcoxon signed-rank tests to assess statistical significance of paired
297 day-night fluxes. Additionally, we compared dawn (0500 to 0700) and dusk (1700 to 1900)
298 median EC measured fluxes using the same methods.

299 Ice coverage at FCR is episodic and ephemeral, encompassing longer ice-covered periods
300 as well as shorter-duration ice-covered periods when ice may be present during portions of
301 sequential days or with partial coverage of the reservoir's surface, which we refer to as
302 intermittent ice-on periods. To explore the role of variable winter ice cover on CO₂ and CH₄
303 fluxes, we analyzed mean half-hourly fluxes (± 1 S.D.) from 10 January to 10 February for both
304 2021 and 2022, which encompassed a period of intermittent (2021) and continuous (2022) ice-on
305 (following Carey and Breef-Pilz 2022; Table S1). We used Mann-Whitney-Wilcoxon tests to
306 determine statistically-significant differences ($\alpha = 0.05$) between the median half-hourly fluxes
307 measured during intermittent and continuous ice-on periods.

308 Finally, we calculated the net annual flux balance for CO₂ and CH₄ using both measured
309 and gap-filled half-hourly EC data. Fluxes were summed across each year (01 May - 30 April).
310 The standard deviation (± 1 S.D.) was calculated for the measured and gap-filled data using the
311 different u^* scenarios. Briefly, half-hourly fluxes were gap-filled in REddyProc using the
312 marginal distribution sampling method (MDS), which uses the correlation of measured fluxes
313 with environmental driver variables, namely, light, moisture, and temperature to estimate fluxes
314 during the missing periods (Wutzler et al. 2018). Gap-filling was performed for each of the u^*
315 scenarios, providing information about the uncertainty that might be introduced to the data by
316 choosing a u^* threshold.

317 2.6 Time series analysis

318 To identify key environmental predictors and test mechanistic relationships between
319 observed mean daily, weekly, and monthly measured CO₂ and CH₄ fluxes and environmental

320 variables, we developed separate autoregressive integrated moving average (ARIMA) models for
321 each timescale. ARIMA models are used to identify key environmental predictors while
322 accounting for temporal autocorrelation (Hyndman and Athanasopoulos, 2018). We selected
323 several potential environmental predictors, including: surface water temperature (Temp, 0.1 m,
324 °C); the difference between surface (0.1 m) and bottom (9 m) water temperatures (Diff. Temp);
325 buoyancy frequency (N^2); thermocline depth (TD); DO percent saturation (DO sat); Chl-*a*;
326 fDOM; and discharge (Inflow) measured at the primary inflow to FCR (Fig. S2, S3). Prior to
327 ARIMA modeling, we conducted pairwise Spearman correlations on all predictor variables
328 (aggregated to each time scale) and removed collinear variables (Pearson's $\rho \geq 0.7$) that were
329 the least correlated with fluxes. N^2 and Diff. Temp were removed for all time scales due to their
330 strong correlation with surface water temperature (Table S2). Response and predictor variables
331 were checked for skewness, transformed if appropriate, and normalized (z-scores) prior to model
332 fitting (Hounshell et al. 2022).

333 We used a model selection algorithm (Lofton et al. 2022) to identify the importance of
334 environmental predictor variables at each time scale. The algorithm was based on the `auto.arima`
335 function in the `forecast` package in R (Hyndman and Khandakar, 2008; Hyndman et al. 2021)
336 which compared fitted models to a global model (all possible predictors) and a null persistence
337 model with just one autoregressive term (AR(1)). We selected the environmental model with the
338 lowest corrected Akaike information criterion (AICc), as well as models within 2 AICc units
339 (Burnham and Anderson, 2002). Models were limited to include one autoregressive term
340 (Hounshell et al. 2022).

341

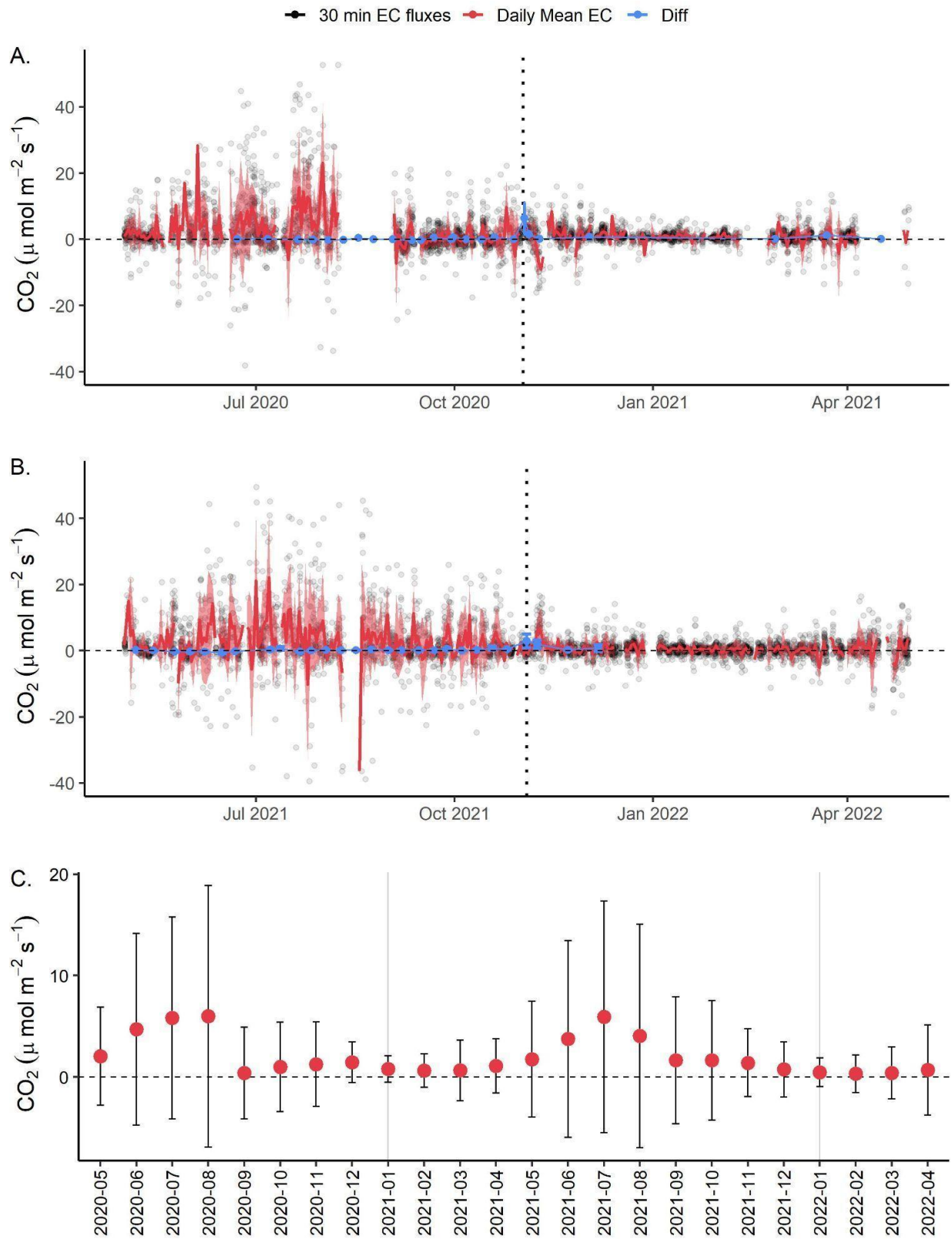
342 **3 Results**

343 Overall, due to data processing and filtering described above, including the 90% footprint
344 restriction, EC fluxes captured 23% and 19% of total CO₂ and CH₄ fluxes, respectively, over two
345 years from FCR (Table S3), which is similar to previously-reported deployments of EC systems
346 at lakes and reservoirs (e.g., Golub et al. 2021; Reed et al. 2018; Waldo et al. 2021). The
347 percentage of available data was relatively consistent across the daily timescale (from 0000 to
348 2330), ranging from 14%-34% of data availability for CO₂ (2200 and 1230, respectively) and

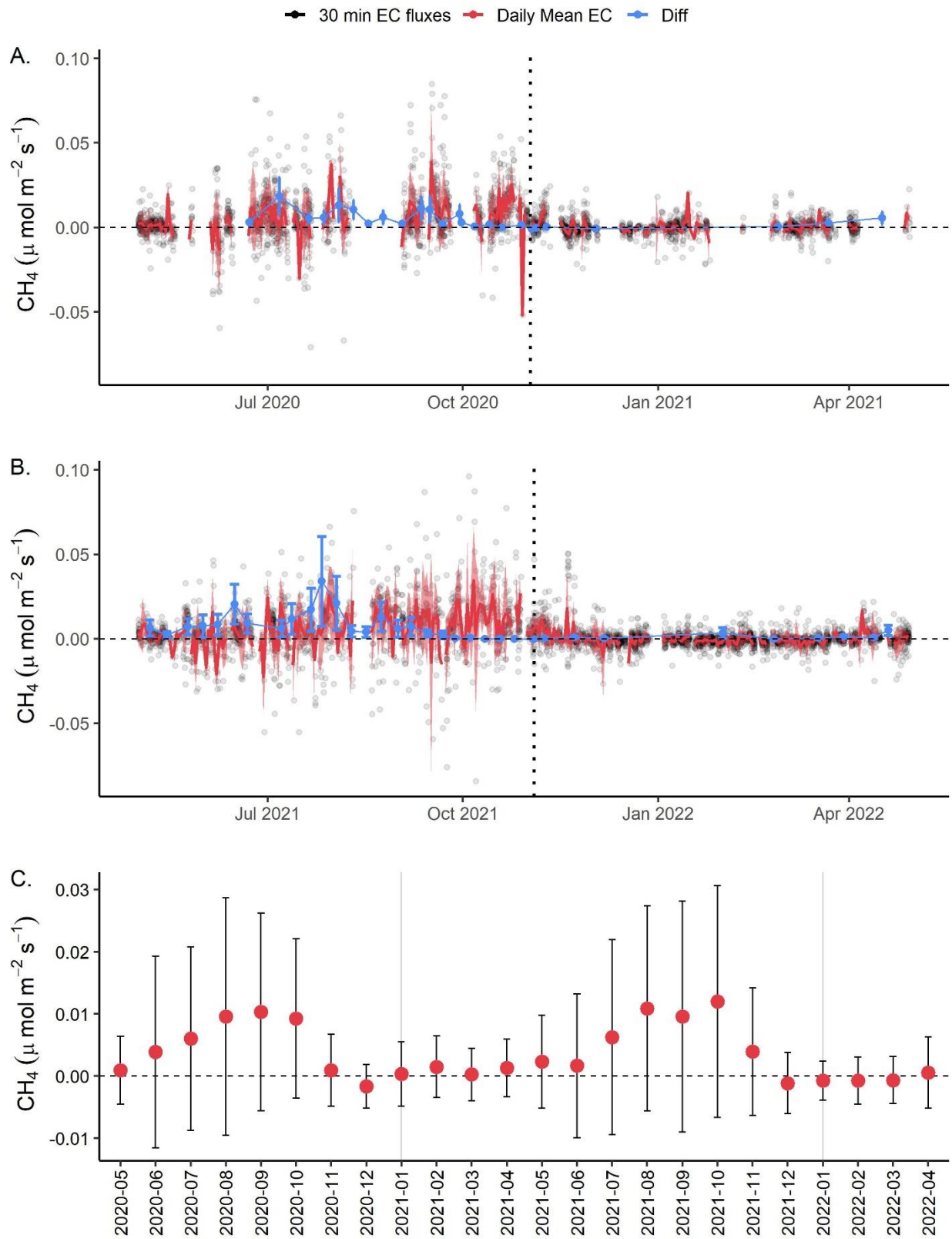
349 11%-32% for CH₄ (2200 and 1230, respectively; Fig. S4). We note that during the day, the
350 dominant wind direction was outside the reservoir footprint, while the dominant wind direction
351 was largely along the reservoir at night (Fig. S5). This pattern resulted in a high percentage of
352 daytime fluxes removed due to wind direction, but overall, we observed a roughly equal
353 contribution of day and night fluxes following all flux removal processes (i.e., flux filtering due
354 to low u*). Data availability after filtering was also relatively consistent throughout seasons and
355 between years, ensuring even representation of measured fluxes throughout the year (Fig. S6).
356 We do note low data availability (<10%) for both CO₂ and CH₄ during August 2020, due to
357 instrument maintenance, and for CH₄ during December 2020 and February 2021.

358 3.1 Phenology of CO₂ and CH₄ fluxes

359 High-frequency EC data show that FCR was generally a net source of both CO₂ and CH₄
360 to the atmosphere throughout the study period (Figs. 2, 3, S7; Tables S4). Overall, measured CO₂
361 fluxes ranged from -39.46 to 52.67 μmol m⁻² s⁻¹ with a mean flux of 1.86 ± 6.21 μmol m⁻² s⁻¹ (±1
362 S.D.) aggregated over the entire 2-year study period. Measured CH₄ fluxes ranged from -0.084 to
363 0.096 μmol m⁻² s⁻¹, with a mean CH₄ flux of 0.003 ± 0.011 μmol m⁻² s⁻¹ over the study period
364 (Fig. 2, 3, S7; Table S4).

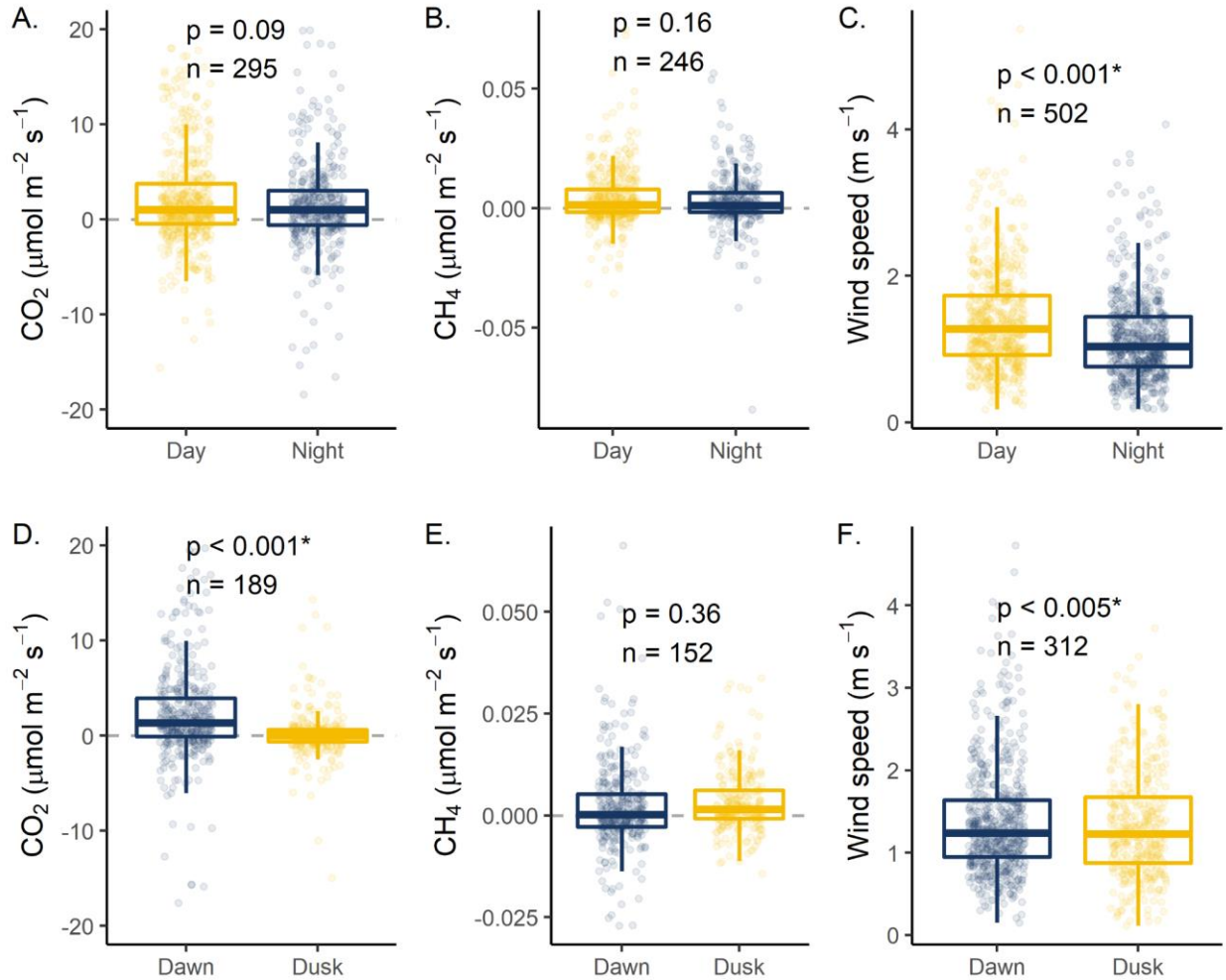


366 **Figure 2.** Daily mean carbon dioxide fluxes (CO_2 , $\mu\text{mol m}^{-2} \text{s}^{-1}$) for A. May 2020 to April 2021
367 (Year 1) and B. May 2021 to April 2022 (Year 2) measured using eddy covariance (Daily Mean
368 EC, red) and calculated discrete diffusive fluxes (Diff, blue) using the mean and standard
369 deviation of seven gas transfer coefficient models (k ; Winslow et al. 2016b). Grey dots represent
370 measured half-hourly fluxes from the EC. The dark red line represents daily mean fluxes. The
371 shaded red area represents ± 1 standard deviation of the daily 30-minute fluxes using measured
372 EC fluxes. The vertical dotted line indicates reservoir fall turnover. C. Mean monthly CO_2 fluxes
373 ($\mu\text{mol m}^{-2} \text{s}^{-1}$) aggregated from measured EC data. The error bars correspond to ± 1 S.D. of
374 aggregated fluxes for both measured and gap-filled EC values. The horizontal dashed line
375 indicates zero fluxes.



377 **Figure 3.** Daily mean methane fluxes (CH_4 , $\mu\text{mol m}^{-2} \text{s}^{-1}$) for A. May 2020 to April 2021 (Year
378 1) and B. May 2021 to April 2022 (Year 2) measured using eddy covariance (Daily Mean EC,
379 red) and calculated discrete diffusive fluxes (Diff, blue) using the mean and standard deviation of
380 seven gas transfer coefficient models (k ; Winslow et al. 2016b). Grey dots represent measured
381 half-hourly fluxes from the EC. The dark red line represents daily mean fluxes. The shaded red
382 area represents ± 1 standard deviation of the daily 30-minute fluxes. The vertical dotted line
383 indicates reservoir fall turnover for each year. C. Mean monthly CH_4 fluxes ($\mu\text{mol m}^{-2} \text{s}^{-1}$)
384 aggregated from measured EC data. The error bars correspond to ± 1 S.D. of aggregated fluxes
385 for both measured and gap-filled EC values. The horizontal dashed line indicates zero fluxes.

386 At the hourly to diel scale, we found that certain times of day had higher fluxes than
387 others, but that overall, there was little difference in fluxes at midday versus midnight. Measured
388 EC fluxes revealed no statistically significant difference between paired CO_2 fluxes measured
389 during the day (1100 to 1300) as compared to night (2300 to 0100; $p=0.09$; Fig. 4; Table S5),
390 and no statistically significant difference between paired, measured day and night CH_4 fluxes
391 ($p=0.16$; Fig. 4; Table S5). We did observe significantly higher median CO_2 fluxes measured at
392 dawn (0500 to 0700; $1.34 \mu\text{mol m}^{-2} \text{s}^{-1}$) as compared to dusk (1700 to 1900; $-0.030 \mu\text{mol m}^{-2} \text{s}^{-1}$;
393 $p<0.001$; Fig 4; Table S5), which may be related to higher median dawn wind speeds ($p<0.001$),
394 though there was no statistical difference between dawn and dusk CH_4 fluxes.



395

396 **Figure 4.** Day (1100 to 1300) vs. night (2300 to 0100) comparisons of A. carbon dioxide (CO₂,
 397 $\mu\text{mol m}^{-2} \text{s}^{-1}$), B. methane (CH₄, $\mu\text{mol m}^{-2} \text{s}^{-1}$), and C. wind speed (m s^{-1}) measured using the
 398 eddy covariance (EC) system deployed at Falling Creek Reservoir. Points represent measured
 399 half-hourly fluxes, while the boxes represent the 25th and 75th percentile, respectively and the
 400 thick line shows the median flux calculated with measured EC data. Dawn (0500 to 0700) vs.
 401 dusk (1700 to 1900) comparisons of D. CO₂, E. CH₄, and F. wind speed. Wilcoxon signed-rank
 402 tests were used to determine statistical significance between paired (day to night; dawn to dusk)
 403 measurements. Statistical significance was defined a priori as $p < 0.05$; asterisks indicate
 404 statistically significant differences. n indicates the number of paired measurements (Table S5).
 405 For CO₂ (A. and B.) some outliers were omitted for data presentation but retained for analysis.

406 At the seasonal scale, both CO₂ and CH₄ fluxes (EC and diffusive measured fluxes) were
 407 greater in magnitude and more variable during the summer than winter, with increasing fluxes
 408 during the late spring and decreasing fluxes during the late fall (Figs. 2, 3). During the summer
 409 months (June – August), FCR was an overall source of CO₂ and CH₄ to the atmosphere for both

410 years (Figs. 2, 3). Specifically, CO₂ and CH₄ fluxes were up to 5× and 15× greater, respectively,
411 during the summer stratified period (May – October) as compared to the winter and early spring
412 (November – April; Fig. 5, S8). During fall turnover, EC measured CO₂ fluxes remained low in
413 both years (2020, 2021), while diffusive fluxes showed an increase in CO₂ fluxes on the day of
414 turnover (Figs. 2, S9). Similarly, CH₄ fluxes were also low during and following turnover for
415 both EC and diffusive fluxes in both years (Figs. 3, S9). From September to April, FCR was a
416 small CO₂ source, but emitted less CO₂ than during the summer. For CH₄, FCR was almost net
417 neutral from late fall to early spring (November to April), in contrast to larger CH₄ emissions
418 during the summer. Following spring mixing, there was a small, but notable increase in CO₂
419 emissions in 2021 but little change in CH₄. In 2022, there were no notable changes in either CO₂
420 or CH₄ following ice-off and subsequent spring mixing in 2022 (Fig. 6). At the annual scale,
421 there were notably higher CO₂ fluxes in the late-summer and early fall 2021 as compared to the
422 summer and fall 2020, while for CH₄, there were notably higher fluxes both in the mid-summer
423 2021 and in the late-summer and early fall 2021 (Figs. 2, 3).

424 3.2 Comparison of EC and diffusive fluxes

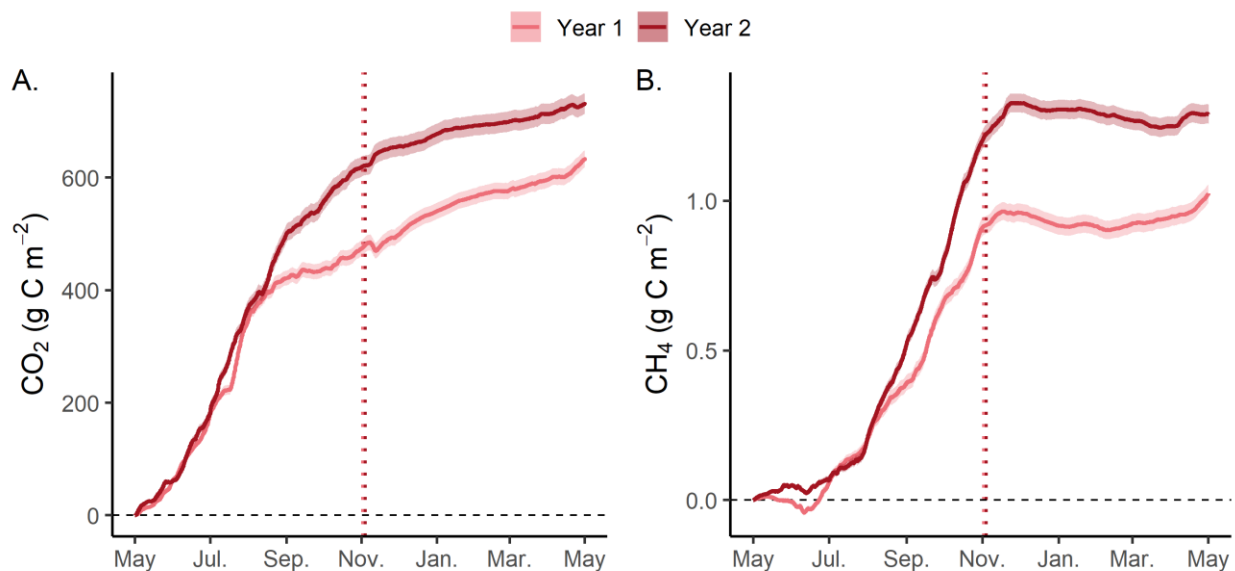
425 Overall, both CO₂ and CH₄, diffusive fluxes were within the range of measured EC
426 fluxes, though diffusive CO₂ fluxes were lower than measured EC fluxes when comparing
427 discrete timepoints (Fig. 2, 3; Table S4). Specifically, hourly CO₂ diffusive fluxes calculated
428 from grab surface samples were an order of magnitude lower than measured EC fluxes and
429 ranged from -1.24 to 17.50 μmol m⁻² s⁻¹, with a mean flux of 0.39 ± 1.29 μmol m⁻² s⁻¹ (Figs. 2,
430 S10, S11; Table S4). We note that the magnitude of diffusive fluxes was highly sensitive to the
431 gas transfer coefficient method (k) used in flux calculations, and thus we present the mean and
432 standard deviation of the seven different k methods used (Eq. 1; Fig. S10). Hourly CH₄ diffusive
433 fluxes were more comparable to measured EC fluxes, with a range of -0.003 to 0.096 μmol m⁻² s⁻¹
434 ¹ and a mean of 0.006 ± 0.009 μmol m⁻² s⁻¹ (Figs. 3, S10, S11; Table S4).

435 3.3 Net CO₂ and CH₄ balance for a small, eutrophic reservoir

436 Gap-filled CO₂ and CH₄ half-hourly fluxes summed across the entire year indicate that
437 FCR was an overall source of CO₂ and CH₄ to the atmosphere (Fig. 5). According to gap-filled
438 EC fluxes, FCR released 633 and 731 g CO₂-C m⁻² year⁻¹, during the first and second years of the

439 study, respectively. For gap-filled CH₄ fluxes, FCR released 1.02 and 1.29 g CH₄-C m⁻² year⁻¹,
440 respectively. The gap-filled and measured data yielded similar estimates when the gap-filled data
441 were scaled by the percentage of missing data from the measured time series (Fig. S12).

442 The annual GHG balances were driven by large fluxes of CO₂ and CH₄ during the
443 summer. Net emissions during the warmest months (June – September; 375 and 496 g CO₂-C m⁻²
444 for year 1 and year 2, respectively) represented up to 68% of the total annual net CO₂ flux as
445 compared to the coldest months (December – March) when only 98 and 57 g CO₂-C m⁻² was
446 emitted (up to 15% of the total annual CO₂). Similarly, for CH₄, up to 66% of the total annual net
447 CH₄ flux was released during the warmest months (June – September; 0.67 and 0.76 g CH₄-C m⁻²
448 ²) and less than 1% during the coldest months (December – March). For the second year of
449 monitoring, annual fluxes were greater for both CO₂ and CH₄, largely due to elevated fluxes in
450 early and late fall (September – November). Cumulatively, the amount of CO₂-C released from
451 FCR was three orders of magnitude greater than the mass of CH₄-C released.



452
453 **Figure 5.** Annual cumulative fluxes using measured and gap-filled eddy covariance (EC) data
454 for A. carbon dioxide (CO₂, g C m⁻²) and B. methane (CH₄, g C m⁻²) using measured and gap-
455 filled EC fluxes from Falling Creek Reservoir for Year 1 (May 2020-April 2021; pink) and Year
456 2 (May 2021-April 2022; dark red). Shaded areas correspond to the aggregated standard
457 deviation (± 1 S.D.) of measurements. The horizontal dashed line corresponds to zero and the
458 vertical dotted line indicates reservoir fall turnover for both years.

459 3.4 Environmental predictors of CO₂ and CH₄ fluxes

460 During the study period, FCR experienced typical meteorological and environmental
461 conditions. The meteorology measured at the reservoir dam recorded a mean air temperature of
462 14.1°C (13.8 and 14.4°C in years 1 and 2, respectively), with a minimum and maximum
463 temperature of -11.5 and 35.1°C, respectively across the two years (Table S6). Mean wind speed
464 during the time period was 1.99 m s⁻¹ (2.00 and 1.97 m s⁻¹ for years 1 and 2, respectively), with a
465 maximum wind speed of 11.2 m s⁻¹ and a dominant wind direction of 198° (191° and 199° for
466 years 1 and 2, respectively). Yearly total rainfall ranged from 790 mm (Year 2) to 1438 mm
467 (Year 1). During the winter (January - February), air temperatures in year 1 ranged from -8.0 to
468 19.4°C with a mean of 1.9°C and in year 2 ranged from -11.5 to 21.4°C with a mean of 2.1°C.

469 Water column variables also exhibited typical annual patterns and were for the most part
470 similar between years. We found surface water temperatures ranged from 1.23 to 31.4°C, with a
471 mean of 15.2 and 15.9°C for years 1 and 2, respectively (Fig. S2; Table S7). Chl-a values ranged
472 from 0.25 to 121 µg L⁻¹, with a mean of 11.5 µg L⁻¹ and 12.3 µg L⁻¹ in years 1 and 2,
473 respectively. fDOM was also nearly identical in years 1 and 2 with a mean of 6.09 and 6.04
474 RFU, respectively, and a range of 3.01 to 10.4 RFU. For DO sat., the mean was 107 and 97.8%
475 in year 1 and year 2. Finally, inflow was higher in year 1 (0.056 m³ s⁻¹) as compared to year 2
476 (0.013 m³ s⁻¹) and ranged from 0.005 to 0.27 m³ s⁻¹ (Fig. S2; Table S7).

477 Overall, surface water temperature and thermocline depth were found to be the most
478 important environmental predictors for both CO₂ and CH₄ fluxes over all timescales analyzed
479 (daily, weekly, monthly), followed by fDOM (Table 1). Inflow discharge was only intermittently
480 important for CO₂ and CH₄ fluxes at various timescales while DO sat. and Chl-a were only
481 intermittently important for CO₂ fluxes (Tables 1, S8). Water temperature was positively
482 correlated with both CO₂ and CH₄ fluxes at all timescales, following the pattern of higher GHG
483 fluxes during summer as compared to winter in the time series data (Figs. 2, 3). CO₂ was
484 negatively associated with thermocline depth while CH₄ was positively associated with
485 thermocline depth at all timescales (Table 1); i.e., CO₂ fluxes were greater when there were

486 shallower thermocline depths, whereas CH₄ fluxes were greater when there were deeper
487 thermocline depths.

488 In addition to water temperature and thermocline depth, CO₂ was positively associated
489 with fDOM across all timescales, while CH₄ was only positively associated with fDOM at the
490 daily and weekly timescales (Table 1). Conversely, inflow was positively associated with CO₂ at
491 daily and weekly timescales, while inflow was negatively associated with CH₄ at weekly and
492 monthly timescales. Finally, Chl-a was negatively associated with CO₂, but only on the daily
493 timescale and was negatively associated with DO sat. at the weekly timescale. CH₄ was not
494 associated with either Chl-a or DO sat. at any timescale.

495 CO₂ fluxes were best predicted by ARIMA models at the monthly timescale
496 (RMSE=0.48 μmol m⁻² s⁻¹), with descending RMSE for the weekly (0.63 μmol m⁻² s⁻¹) and then
497 daily (0.97 μmol m⁻² s⁻¹) models (Tables 1; S8). For CH₄, the best-fitting ARIMA model was
498 also identified at the monthly timescale (RMSE=0.41 μmol m⁻² s⁻¹), with descending RMSE for
499 the weekly and daily models ranging from 0.64 and 1.02 μmol m⁻² s⁻¹, respectively (Tables 1,
500 S8). Full ARIMA results are reported in Table S8.

501 **Table 1.** *Best-fit results from Autoregressive Integrated Moving Average (ARIMA) analysis*

GHG	Timescale	Model Order	Surface Temp (°C)	DO Sat. (%)	Chl-a ($\mu\text{g L}^{-1}$)	fDOM (RFU)	Inflow ($\text{m}^3 \text{s}^{-1}$)	Thermo. Depth (m)	RMSE ($\mu\text{mol m}^2 \text{s}^{-1}$)
CO2	Daily	(1,0,0)	0.18	-	-0.17	0.07	0.08	-0.09	0.97
	Weekly	(0,0,0)	0.64	-0.16	-	0.13	0.20	-0.19	0.63
	Monthly	(0,0,0)	0.73	-	-	0.24	-	-0.31	0.48
CH4	Daily	(0,0,0)	0.27	-	-	0.12	-	0.25	1.02
	Weekly	(0,1,1)	0.36	-	-	0.23	-0.36	0.24	0.64
	Monthly	(0,0,1)	0.74	-	-	-	-0.26	0.21	0.41

502

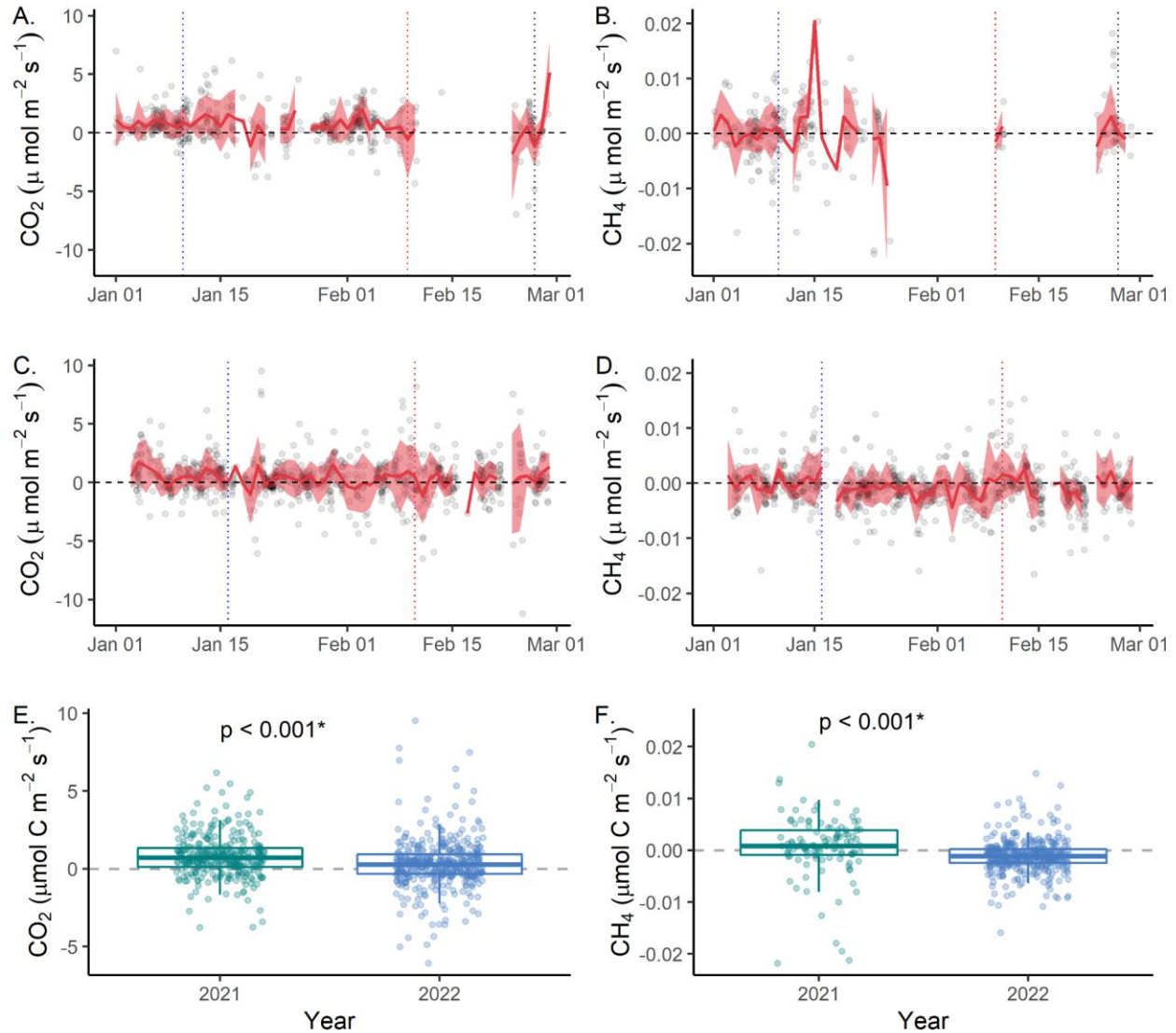
503 *Note:* Table includes only the top selected model (lowest corrected Akaike Information Criterion, AICc). Models are separated by
 504 greenhouse gas (GHG) flux as carbon dioxide (CO₂) and methane (CH₄) as well as by timescale (daily, weekly, monthly).

505 Environmental predictors included: Surface temperature (Surface Temp, °C), dissolved oxygen saturation (DO Sat, %), Chlorophyll-*a*
 506 (Chl-*a*, $\mu\text{g L}^{-1}$), fluorescent dissolved organic matter (fDOM, RFU), inflow discharge (Inflow, $\text{m}^3 \text{s}^{-1}$), and thermocline depth
 507 (Thermo. Depth, m). Model order is specified as (p,d,q) where p is the order of the AR term, d is the order of the integration term, and
 508 q is the order of the MA term. For brevity, the autoregressive (AR) and moving average (MA) terms have been removed but can be
 509 found in the supplemental information. Results for all models with 2 AICc of the best fitting model, can be found in the supplemental
 510 information (Table S8). Dashed lines indicate environmental parameters that were not identified as statistically significant. The root
 511 mean square error (RMSE) is reported for each model. Standard errors for each parameter value are given in Table S8.

512 3.5 Influence of ice cover on CO₂ and CH₄ fluxes

513 FCR experienced two distinct winter regimes in 2021 vs. 2022. In 2021, ice-on first
514 occurred on 10 January 2021, then came on and off multiple times before final ice-off on 23
515 February 2021. Overall, there were 27 days with some ice and 9 days with some open-water
516 during the 2021 intermittent ice-period. In contrast, in 2022, there was near-continuous ice cover
517 from 10 January to 10 February, with ice-on occurring from 16 January 2022 and final ice-off on
518 10 February 2022. While we were unable to collect ice thickness data through both winters due
519 to safety concerns, peak ice thickness in FCR in 2022 was ~9.5 cm whereas peak ice thickness in
520 2021 was ~2 cm.

521 When comparing measured half-hourly fluxes aggregated across the intermittent ice-on
522 period in winter 2021 and the continuous ice-on period in winter 2022, there were statistically-
523 significantly higher median CO₂ and CH₄ fluxes measured during intermittent ice-on than
524 continuous ice-on (Kruskal-Wallis $p < 0.0001$; Fig. 6; Table S9). During intermittent ice-on in
525 winter 2021, median CO₂ fluxes were 0.71 $\mu\text{mol m}^{-2} \text{s}^{-1}$, 2.5 \times higher than the median of 0.28
526 $\mu\text{mol m}^{-2} \text{s}^{-1}$ during continuous ice-on in 2022. For CH₄, median fluxes were 0.001 $\mu\text{mol m}^{-2} \text{s}^{-1}$
527 and -0.001 $\mu\text{mol m}^{-2} \text{s}^{-1}$, during intermittent ice-on and continuous ice-on, respectively (Table
528 S9). Throughout the winter period, mean daily CO₂ and CH₄ fluxes were much lower and less
529 variable than in the summer, for both years (Fig. 2, 3).



530

531 **Figure 6.** Mean daily fluxes during the winter of 2021 for A. Carbon dioxide (CO₂, μmol m⁻² s⁻¹)
 532 and B. Methane (CH₄ μmol m⁻² s⁻¹) during intermittent ice-on. Mean daily fluxes during winter
 533 of 2022 for C. CO₂ and D. CH₄ during continuous ice-on. Grey dots represent measured half-
 534 hourly fluxes while the solid red line indicates mean daily fluxes. The shaded red area
 535 corresponds to the standard deviation (±1 S.D.) of the daily mean fluxes. The blue vertical
 536 dashed lines correspond to the start of either intermittent or continuous ice-on for winter 2021
 537 and 2022, respectively, while the red vertical dashed lines correspond to the start of complete
 538 ice-off. The black dashed line in 2021 corresponds to spring mixing (first day after ice-off when
 539 the temperature at 1 m and 8 m was < 1°C). For 2022, spring mixing was on the same day as ice-
 540 off. Boxplots of measured E. CO₂ and F. CH₄ fluxes during each winter's intermittent or
 541 continuous ice-on, respectively. For each box plot, the median is represented as the bold line
 542 while the 25th and 75th percentiles are represented as the bottom and top of the box, respectively.
 543 The whiskers represent minimum and maximum values (1.5× interquartile range). Points
 544 represent all half hourly fluxes measured during the respective winter intermittent or continuous
 545 ice-on, respectively period. The dashed horizontal line corresponds to zero fluxes. Asterisks

546 indicate statistically significant differences between median half-hourly fluxes measured during
547 intermittent (2021) and continuous (2022) ice-on periods using Mann-Whitney-Wilcoxon tests (α
548 = 0.05).

549

550 **4 Discussion**

551 This study provides the first annual-scale, multi-year estimates of both CH₄ and CO₂
552 fluxes using an EC system from a small reservoir. While using EC systems in small freshwaters
553 is inherently challenging and contains several limitations, our work reveals variable patterns in
554 both CH₄ and CO₂ fluxes over sub-daily to seasonal scales. Our study was limited by low levels
555 of measured data, underscoring the need for more accurately quantifying the GHG contributions
556 of small reservoirs on multiple timescales. Despite these challenges, however, our data suggest
557 that FCR was a substantial CO₂ and CH₄ source to the atmosphere. Below we discuss some of
558 the challenges of using an EC system in small freshwaters as well as the patterns and potential
559 drivers of variability in fluxes (CO₂ and CH₄) over multiple timescales. We also discuss the role
560 of various environmental parameters in constraining GHGs fluxes, including during winter ice-
561 cover in small, temperate systems.

562 4.1 Variability in sub-daily fluxes, with higher dawn than dusk CO₂ fluxes

563 A key advantage of an EC system is the ability to capture variability in sub-daily GHG
564 fluxes throughout the year. Despite data gaps and limitations, the fluxes collected by the EC
565 represent a substantial increase in the ability to identify variability in fluxes at multiple
566 timescales. Our work complements previous studies of freshwater systems using EC
567 measurements that observed high sub-daily variability in both summer CO₂ (Liu et al. 2016;
568 Golub et al. 2021; Shao et al. 2015) and CH₄ fluxes (Eugster et al. 2011; Podgrajsek et al. 2014;
569 Taoka et al. 2020; Waldo et al. 2021) and furthers our understanding of the variability of CO₂
570 and CH₄ fluxes on multiple timescales.

571 When comparing day (1100 to 1300) versus night (2300 to 0100) fluxes, we observed no
572 statistically significant differences between CO₂ or CH₄ fluxes during the day as compared to
573 night using measured EC fluxes aggregated over the full year (Fig. 4). Similarly, studies in two
574 small Finnish lakes also found no evidence for diel differences in CO₂ fluxes (Erkkilä et al.

575 2018; Mammarella et al. 2015), while Waldo et al. (2021) found diel differences in CH₄ fluxes
576 on only 18.5% of days out of a 2-year study period. Other studies, however, have observed more
577 consistent diel patterns in GHG fluxes. For example, some studies have shown higher CH₄ fluxes
578 during the night in lakes and reservoirs (Eugster et al. 2011; Podgrasjek et al. 2014; Waldo et al.
579 2021) and higher CO₂ fluxes at night in streams (Attenmeyer et al. 2021; Gómez-Gener et al.
580 2021). On the other hand, some studies observed higher CH₄ fluxes during the day as compared
581 to night (Erkkilä et al. 2018; Jammet et al. 2017; Podgrasjek et al. 2016; Siczko, et al. 2020).
582 Clearly, there is a range of responses to diel variation among lake and reservoir CO₂ and CH₄
583 fluxes, and more work is needed to identify when, where, and why lakes and reservoirs may emit
584 differential GHGs during day vs. night.

585 While we did not observe statistically significant differences between GHG fluxes
586 measured during the day as compared to night, we did observe statistically significantly higher
587 CO₂ fluxes at dawn (0500 to 0700) as compared to dusk (1700 to 1900), but no difference in
588 dawn vs. dusk CH₄ fluxes (Fig. 4). Similarly, studies conducted in other lakes also found CO₂
589 flux minima during the late afternoon (~1800) and CO₂ flux maxima during the early morning
590 (~0600; Liu et al. 2016; Shao et al. 2015), supporting our observations of higher dawn CO₂
591 fluxes. Liu et al. (2016) hypothesized the lower CO₂ fluxes observed during the day (~1800)
592 were likely a result of elevated primary productivity during the afternoon, primarily in the
593 summer months, but could have also been due to convective mixing at night.

594 Altogether, our results provide additional evidence that the time of sample collection has
595 important implications for upscaling freshwater GHG fluxes to longer timescales (Attenmeyer et
596 al. 2021; Gómez-Gener et al. 2021). A previous study conducted in FCR which estimated CO₂
597 and CH₄ diffusive fluxes using discrete GHG measurements only collected at ~noon concluded
598 FCR was often a small CO₂ sink during the summer stratified period in 2015-2016 (McClure et
599 al. 2018), whereas our diel EC data indicate that FCR was an overall CO₂ source throughout the
600 summer in both 2020 and 2021. While the flux magnitudes measured by McClure et al. (2018)
601 were similar to the present study, the overall conclusions were different due to the temporal
602 resolution of sample collection.

603 4.2 Important role of water temperature and thermocline depth in constraining daily,
604 weekly, and monthly CO₂ and CH₄ fluxes

605 Following our analysis of CO₂ and CH₄ fluxes over daily to seasonal timescales, we then
606 used time-series analysis to test the potential effects of various environmental variables on GHG
607 fluxes. Specifically, ARIMA results show that surface water temperature was positively
608 correlated with both CO₂ and CH₄ fluxes at the daily, weekly, and monthly timescales (Table 1).
609 These results were supported by higher fluxes of both CO₂ and CH₄ observed during the warmer
610 summer months when aggregated to daily, weekly, and monthly timescales (Fig. 2, 3, S7).
611 Strong positive correlations between GHG fluxes (both CO₂ and CH₄) and water temperature
612 have been observed in several freshwater ecosystems, especially on longer timescales, with clear
613 differences between summer and winter fluxes (monthly to seasonally; Eugster et al. 2011; Reed
614 et al. 2018; Taoka et al. 2020).

615 In addition to temperature, thermocline depth was also identified as an important
616 environmental parameter controlling both CO₂ and CH₄ fluxes. For CO₂, thermocline depth was
617 negatively associated with fluxes at all timescales, indicating higher CO₂ fluxes when the
618 thermocline was shallower. Generally, thermocline depth was shallower in the late summer (Fig.
619 S3) when CO₂ fluxes were observed to be greatest and most variable in FCR. This pattern may
620 be indirectly related to water temperature, as shallower thermocline depths were weakly
621 negatively associated with warmer water temperatures, and there was a strong positive
622 relationship between CO₂ fluxes and water temperature, as discussed above.

623 Conversely, thermocline depth was positively correlated with CH₄ at all timescales
624 (daily, weekly, monthly), indicating higher CH₄ fluxes when the thermocline depth was deeper,
625 which was generally observed during the late spring and early summer (Fig. S3). Previous
626 studies have suggested water column mixing is an important control on CH₄ fluxes, leading to
627 higher fluxes during convective and wind-driven mixing when high concentrations of CH₄
628 accumulated in the deeper waters are mixed to the surface, which would be more common when
629 the thermocline depth is deeper (Sieczko et al. 2021). In addition, we hypothesize this
630 relationship may also be due to the contribution of ebullition to total CH₄ fluxes, which has
631 shown to be a small but important component of CH₄ fluxes near the deepest point of FCR,

632 where the EC system was deployed (McClure et al. 2020). We might expect ebullition to provide
633 a greater percentage of overall emissions when the thermocline is deeper, though additional
634 research is needed to confirm this mechanism.

635 Following temperature and thermocline depth, fDOM was identified as a key positive
636 environmental predictor for CO₂ fluxes at all timescales (daily, weekly, monthly; Table 1). A
637 similar positive relationship between terrestrially-derived DOM and dissolved CO₂ was
638 identified in 48 Canadian streams (D'Amario and Xenopoulos, 2015). As fDOM sensors are
639 thought to mainly capture allochthonous DOM (Howard et al. 2021; Watras et al. 2015), this
640 finding suggests that allochthonous DOM from the reservoir's primary inflow stream or diffuse
641 overland flow may result in elevated CO₂ emissions from freshwater ecosystems. This follows
642 previous research which has identified allochthonous carbon inputs and associated DOC
643 concentrations as important predictors of CO₂ fluxes in lakes (Sobek et al. 2005). Unlike for
644 CO₂, fDOM was only identified as an important environmental predictor for CH₄ fluxes at
645 shorter timescales (daily, weekly). In an analysis of >300 lakes, Sanches et al. (2019) found a
646 strong positive relationship between dissolved organic C and diffusive CH₄ fluxes, suggesting
647 dissolved organic C may play an important role in constraining CH₄ fluxes across multiple lakes
648 and timescales. The strong positive correlation between CH₄ fluxes and fDOM observed here
649 further indicates that dissolved organic C, as a proxy from fDOM (Howard et al. 2021), may also
650 be important at the local scale on short-timescales.

651 In addition to these overarching patterns, several environmental parameters were
652 intermittently important for various timescales for either CO₂ or CH₄. CO₂ was positively
653 correlated with inflow at shorter timescales (daily, weekly) while CH₄ was negatively correlated
654 with inflow but only at longer timescales (weekly, monthly; Table 1). Following the positive
655 relationship between CO₂ and fDOM, we hypothesize the positive relationship with inflow
656 reflects the importance of allochthonous DOM delivery to FCR via the primary inflow and
657 diffuse overland flow. Previous research examining CH₄ fluxes from FCR have found similar
658 negative relationships between inflow and CH₄ fluxes, especially via ebullition in the upstream,
659 littoral portion of the reservoir (McClure et al. 2020). Results from this study suggest inflow is
660 similarly correlated with CH₄ fluxes at the deepest point of the reservoir, primarily on longer
661 timescales (weekly, monthly). Finally, Chl-a was negatively associated with CO₂ fluxes at the

662 daily timescale while DO sat. was negatively associated with CO₂ fluxes at the weekly timescale
663 (Table 1). Both of these relationships suggest a coupling between high primary production, as
664 indicated by high Chl-a and high DO Sat., and low CO₂ fluxes on shorter timescales (daily,
665 weekly). Previous studies have identified a weak negative relationship between primary
666 production and CO₂ fluxes on the sub-daily timescale in other eutrophic, freshwater lakes and
667 reservoirs (Liu et al. 2016; Shao et al. 2015).

668 4.3 Role of fall turnover and ice cover in affecting GHG dynamics

669 Contrary to previous studies conducted in both FCR and other thermally-stratified
670 waterbodies (e.g., Erkkilä et al. 2018; McClure et al. 2018; 2020), we observed low CO₂ and
671 CH₄ fluxes during the days surrounding fall turnover for both years (1 November 2020; 3
672 November 2021), when EC data indicate that FCR was a small to negligible CO₂ and CH₄ source
673 (Fig. 2, 3, S9). Discrete diffusive fluxes measured on the day of fall turnover suggest FCR was a
674 4x and 14x larger CO₂ source than fluxes measured with the EC, in years 1 and 2 (Figs. 2, S9).
675 Similar to CO₂, we found the magnitude of CH₄ fluxes decreased following fall turnover but
676 remained a small source (Fig. 3, S9). McClure et al. (2018) observed episodic release of CH₄
677 from FCR during the weeks prior to fall turnover as high concentrations of CH₄ that had
678 accumulated in the middle of the water column were emitted during wind-mixing. In the weeks
679 prior to fall turnover, we did observe elevated CH₄ emissions in both years (Figs. 3, S9),
680 supporting this observed mechanism (McClure et al. 2018), and decreasing the importance of fall
681 turnover as a single pulse of emissions.

682 Importantly, this study provides some of the first near-continuous flux measurements of
683 both CO₂ and CH₄ during winter, including during intermittent and continuous ice-on conditions
684 (Fig. 6). We found significantly higher CO₂ and CH₄ fluxes during intermittent ice-on as
685 compared to continuous ice-on ($p < 0.001$; Fig. 6; Table S9), demonstrating the importance of
686 annually-variable, winter ice dynamics to seasonal GHG fluxes. Of the studies that report GHG
687 fluxes during continuous ice-on, all report low fluxes with low variability (A.K. Baldocchi et al.
688 2020; Jammet et al. 2015, 2017; Reed et al. 2018), similar to the winter with continuous ice-on at
689 FCR. Interestingly, these studies also noted high fluxes immediately following ice-off for both
690 CO₂ and CH₄ (Anderson et al. 1999; A.K. Baldocchi et al. 2020; Gorsky et al. 2021; Jammet et

691 al. 2015, 2017; Podgrajsek et al. 2015; Takoa et al. 2020), which was not observed at FCR.
692 Unlike these previous studies, which were largely conducted in northern lakes which are frozen
693 for months at a time, FCR is a more temperate system which only periodically freezes for a few
694 days to months at time (Carey and Breef-Pilz, 2022). We hypothesize that the brief continuous
695 ice-cover observed at FCR during winter 2022 (25 days) was not long enough to promote
696 extensive accumulation of GHGs under ice, as observed by the other studies. Further work on the
697 effect of ice cover on GHG fluxes is needed, but our comparison of intermittent ice-on vs.
698 continuous ice-on suggests that the increasing intermittent ice-cover being experienced in many
699 lakes worldwide (Imrit and Sharma, 2021; Sharma et al. 2021; Woolway et al. 2020) will likely
700 increase winter GHG fluxes.

701 4.4 Much higher annual CO₂ emissions from FCR than other studied reservoirs

702 When scaling fluxes to the full year, FCR was a much smaller annual CH₄ source (1.02-
703 1.29 g m⁻² yr⁻¹), yet a larger CO₂ source (633-731 g m⁻² yr⁻¹; Figs. 5, S12), than other reservoirs
704 reported in the literature to date (A.K. Baldocchi et al. 2020; Deemer et al. 2016; Golub et al.
705 2021). While the total magnitude of CO₂ emissions from FCR was greater than most studies,
706 Golub et al. (2021) similarly found that data from 12 lakes and reservoirs over multiple years
707 emitted substantial amounts of CO₂ in their synthesis of EC measured CO₂ fluxes in freshwaters
708 (13.6 - 224 g C m⁻² yr⁻¹), except for one reservoir during one year which had a CO₂ flux of -53.6
709 g C m⁻² yr⁻¹. As compared to other reservoirs with GHG flux data, FCR is old (>100 years old)
710 which may lead to lower GHG emissions, particularly CH₄ (Barros et al. 2011; McClure et al.
711 2020; Prairie et al. 2018).

712 Despite its age, however, FCR was a much larger CO₂ source as compared to other lakes
713 and reservoirs. The CO₂ emissions were consistently high among years, suggesting that FCR
714 may be a greater source of CO₂ than most terrestrial environments (-70 to 20 g C m⁻² yr⁻¹ for
715 multi-year, undisturbed terrestrial sites; D.D. Baldocchi et al. 2020). Comparisons between years
716 suggest that slightly higher annual fluxes of CO₂ and CH₄ in the early to late fall (September -
717 November) of the first monitoring year as compared to the second year may be related to slightly
718 higher mean air temperatures or lower inflow levels (and corresponding longer hydraulic
719 residence times), though this remains unknown. We note that these cumulative fluxes are likely

720 conservative, as there were substantial gaps in measured EC fluxes during year 1, particularly in
721 August 2020, likely resulting in underestimated measured fluxes during this time of year when
722 fluxes are usually highest (Fig. 5, S12).

723 4.5 Challenges of using EC systems in small, freshwater lakes and reservoirs

724 While the study described here greatly expands the temporal frequency of measured CO₂
725 and CH₄ fluxes from a small reservoir, several caveats must be taken into consideration. EC
726 systems are notoriously difficult to use in freshwater ecosystems due to footprint considerations
727 (Vesala et al. 2006), frequent occurrences of low u^* values, particularly at night (Vesala et al.
728 2006; Scholz et al. 2021), as well as general considerations resulting in high percentages of data
729 removed due to these and other issues (yielding data coverage of 10 – 40%; e.g., A.K. Baldocchi
730 et al. 2020; Erkkilä et al. 2018; Houtari et al. 2011; Ouyang et al. 2017; Shao et al. 2015; Waldo
731 et al. 2021; Table S3). While low data coverage is common, data gaps were relatively consistent
732 across timescales (daily to seasonally) to ensure unbiased data. Furthermore, compared to the
733 temporal frequency of many grab sample methods (i.e., samples measured weekly, biweekly, or
734 monthly), the data coverage of the EC system is still a substantial improvement and more
735 accurately captures fluxes across multiple timescales challenging to sample, such as at night,
736 during winter ice-cover, and during episodic events, such as fall turnover.

737 While strict filtering processes were enacted to limit non-local fluxes (i.e., filtering fluxes
738 when the along-wind distance providing 90% of the cumulative contribution was outside the
739 reservoir), we are unable to completely rule out potential non-local processes (e.g., land-lake
740 interactions) which occur outside the footprint and are entrained or advected into the EC
741 footprint area (Esters et al. 2020; Vesala et al. 2006, 2011; Fig. S1). These processes may be
742 particularly important in small freshwaters located in mountainous regions (Scholz et al. 2021).
743 Based on studies conducted in similar terrestrial ecosystems, we might expect negative CO₂
744 fluxes in the summer followed by substantial CO₂ emissions in the fall and winter; however,
745 these patterns were not observed in FCR, suggesting the majority of fluxes measured in this
746 study likely originated in the reservoir. When taken into account and interpreted cautiously, the
747 data collected by the EC system provides a far more comprehensive time series than what is
748 possible from discrete measurements (Anderson et al. 1999; Eugster 2003; Houtari et al. 2011;

749 Jonsson et al. 2008; Scholz et al. 2021), which is critical for increasing our understanding of
750 GHG fluxes from small reservoirs on multiple temporal scales.

751 Finally, comparisons with diffusive grab samples suggest fluxes measured with the EC
752 system were consistently higher than those estimated with diffusive grab samples, especially for
753 CO₂ (Fig 2, S11), which is consistent with previous studies (Scholz et al. 2021, and references
754 therein). Conversely, CH₄ fluxes calculated using the discrete diffusive methods were more
755 comparable to those measured by the EC system (Fig. 3, S11). Discrepancies between EC
756 measured fluxes and diffusive grab samples may be a result of the different spatial resolution of
757 the two methods, where the EC system is measuring fluxes both at the deepest point of the
758 reservoir in addition to upstream and littoral portions of the reservoir while diffusive grab
759 samples were only collected at the deepest point of the reservoir (Fig. 1; Scholz et al. 2021).
760 Indeed, several studies have observed higher CO₂ and CH₄ fluxes in the littoral zone, closer to
761 the shore, which would have been encompassed in the measured EC fluxes but not the diffusive
762 grab samples (Erkkilä et al. 2018; McClure et al. 2020; Scholz et al. 2021; Taoka et al. 2020),
763 though additional studies in FCR are needed to confirm this pattern.

764

765 **5 Conclusions**

766 Overall, we observed FCR to be a source of CO₂ and CH₄ to the atmosphere on annual
767 timescales (633-731 g CO₂-C m⁻² yr⁻¹; ~1.02-1.29 g CH₄-C m⁻² yr⁻¹). Importantly, by measuring
768 fluxes near-continuously for a full year, we found winter fluxes (December-March) of both CO₂
769 and CH₄ to be comparatively smaller (15-25% and <1% of total annual fluxes, respectively) than
770 the summer stratified period (June - September) yet still important for annual GHG fluxes. In
771 addition, measuring GHG fluxes during two winters with contrasting ice-cover, showed
772 significantly higher CO₂ and CH₄ fluxes during intermittent as compared to continuous ice-on.
773 Finally, we identified surface water temperature, thermocline depth, and several other
774 environmental variables (fDOM, inflow) as important drivers of both CO₂ and CH₄ fluxes on
775 multiple timescales. Altogether, our results suggest that CO₂ and CH₄ are highly dynamic on

776 multiple temporal scales and highlight the role of small reservoirs as important GHG sources in
777 global budgets.

778

779 **Acknowledgments**

780 This project originated in February 2020 and was made possible through creative teamwork
781 spanning international borders amidst a global pandemic. We thank Bobbie Niederlehner,
782 Bethany Bookout, Heather Wander, Abigail Lewis, Whitney Woelmer, Dexter Howard, Nicholas
783 Hammond, Arpita Das, Ryan McClure, Mary Lofton, and Calvin Thomas for their assistance
784 with field collection and laboratory analysis. Zoran Nesic and Vahid Daneshmand provided
785 critical troubleshooting assistance and technical support. Additionally, we thank the Western
786 Virginia Water Authority (WVWA), especially Jamie Morris, for long-term access to field sites
787 and logistical support. We gratefully acknowledge funding from U.S. National Science
788 Foundation grants CNS-1737424, DEB-1753639, DEB-1926050, DBI-1933102, and DBI-
789 1933016; and Fralin Life Sciences Institute at Virginia Tech. We also acknowledge Discovery
790 Grant support to Johnson provided by the Natural Sciences and Engineering Research Council of
791 Canada (NSERC), RGPIN-2020-06252. The authors report no conflicts of interest.

792

793 **Open Research**

794 The eddy covariance dataset and associated QA/QC code for this study can be found in the
795 Environmental Data Initiative (EDI) repository via
796 <https://doi.org/10.6073/pasta/a1324bcf3e1415268996ba867c636489> and [https://portal-](https://portal-s.edirepository.org/nis/mapbrowse?packageid=edi.920.2)
797 [s.edirepository.org/nis/mapbrowse?packageid=edi.920.2](https://portal-s.edirepository.org/nis/mapbrowse?packageid=edi.920.2) (Carey et al. 2022a). Additionally, code
798 used for the timeseries and ARIMA analyses are archived at <https://10.5281/zenodo.6818141>
799 (Zenodo; Hounshell et al. 2022). Additional datasets including the meteorological data set
800 (<https://portal-s.edirepository.org/nis/mapbrowse?scope=edi&identifier=143&revision=14>,
801 Carey et al. 2022c), limnological dataset
802 (<https://doi.org/10.6073/pasta/81c6c76f4fe22434a20aa8c00f2d4ad1> and [https://portal-](https://portal-s.edirepository.org/nis/mapbrowse?scope=edi&identifier=518&revision=11)
803 [s.edirepository.org/nis/mapbrowse?scope=edi&identifier=518&revision=11](https://portal-s.edirepository.org/nis/mapbrowse?scope=edi&identifier=518&revision=11), Carey et al. 2022d),

804 inflow discharge (<https://doi.org/10.6073/pasta/c65755d4c0102dde6e3140c1c91b77d6> and
805 <https://portal-s.edirepository.org/nis/mapbrowse?packageid=edi.923.1>, Carey et al. 2022e), ice-
806 cover (<https://portal.edirepository.org/nis/mapbrowse?packageid=edi.456.4>, Carey and Breef-
807 Pilz, 2022), and dissolved discrete grab greenhouse gas concentrations
808 (<https://doi.org/10.6073/pasta/2fb836492aace4c13b7962f2718be8e5> and [https://portal-
809 s.edirepository.org/nis/mapbrowse?scope=edi&identifier=928&revision=3](https://portal-s.edirepository.org/nis/mapbrowse?scope=edi&identifier=928&revision=3), Carey et al. 2022b)
810 are also archived in the EDI. All data (2020-2022) are available for review in the EDI staging
811 environment and will be published following manuscript acceptance. All data through 2021 have
812 been published to EDI and are available under the Creative Commons License - Attribution.

813 **References**

- 814 Anderson, D.E., Striegl, R.G., Stannard, D.I., Michmerhuizen, C.M., McConnaughey, T.A., &
815 LaBaugh, J.W. (1999). Estimating lake-atmosphere CO₂ exchange. *Limnology and*
816 *Oceanography*, 44(4), 988–1001. <https://doi.org/10.4319/lo.1999.44.4.0988>
- 817 Attermeyer, K., Casas-Ruiz, J.P., Fuss, T., Pastor, A., Cauvy-Fraunié, S., Sheath, D., et. al.
818 (2021). Carbon dioxide fluxes increase from day to night across European streams.
819 *Communications Earth & Environment*, 2(1), 118. [https://doi.org/10.1038/s43247-021-](https://doi.org/10.1038/s43247-021-00192-w)
820 [00192-w](https://doi.org/10.1038/s43247-021-00192-w)
- 821 Baldocchi, A.K., Reed, D.E., Loken, L.C., Stanley, E.H., Huerd, H., & Desai, A.R. (2020).
822 Comparing spatial and temporal variation in lake-atmosphere carbon dioxide fluxes using
823 multiple methods. *Journal of Geophysical Research: Biogeosciences*, 125(12).
824 <https://doi.org/10.1029/2019JG005623>
- 825 Baldocchi, D.D. (2020). How eddy covariance flux measurements have contributed to our
826 understanding of Global Change Biology. *Global Change Biology*, 26(1), 242–260.
827 <https://doi.org/10.1111/gcb.14807>
- 828 Barros, N., Cole, J.J., Tranvik, L.J., Prairie, Y.T., Bastviken, D., Huszar, V.L.M., del Giorgio, P.,
829 & Roland, F. (2011). Carbon emission from hydroelectric reservoirs linked to reservoir
830 age and latitude. *Nature Geoscience*, 4(9), 593–596. <https://doi.org/10.1038/ngeo1211>
- 831 Bartosiewicz, M., Przytulska, A., Lapierre, J., Laurion, I., Lehmann, M.F., & Maranger, R.
832 (2019). Hot tops, cold bottoms: Synergistic climate warming and shielding effects
833 increase carbon burial in lakes. *Limnology and Oceanography Letters*, 4(5), 132–144.
834 <https://doi.org/10.1002/lol2.10117>
- 835 Bastviken, D., Sundgren, I., Natchimuthu, S., Reyier, H., & Gålfalk, M. (2015). Technical Note:
836 Cost-efficient approaches to measure carbon dioxide (CO₂) fluxes and concentrations in
837 terrestrial and aquatic environments using mini loggers. *Biogeosciences*, 12(12), 3849–
838 3859. <https://doi.org/10.5194/bg-12-3849-2015>

839 Bastviken, D., Tranvik, L.J., Downing, J.A., Crill, P.M., & Enrich-Prast, A. (2011). Freshwater
840 Methane Emissions Offset the Continental Carbon Sink. *Science*, 331(6013), 50–50.
841 <https://doi.org/10.1126/science.1196808>

842 Beaulieu, J.J., DelSontro, T., & Downing, J.A. (2019). Eutrophication will increase methane
843 emissions from lakes and impoundments during the 21st century. *Nature*
844 *Communications*, 10(1), 1375. <https://doi.org/10.1038/s41467-019-09100-5>

845 Burba, G., Schmidt, A., Scott R.L., Nakai, T., Kathilankal, J., Fratini, G., et al. (2012).
846 Calculating CO₂ and H₂O eddy covariance fluxes from an enclosed gas analyzer using an
847 instantaneous mixing ratio. *Global Change Biology*, 18(1), 385-399.
848 <https://doi.org/10.1111/j.1365-2486.2011.02536.x>

849 Burnham, K.P., & Anderson, D.R. (2002). *Model selection and multimodel inference: a practical*
850 *information-theoretic approach*. New York, NY: Springer.

851 Butman, D., Stackpole, S., Stets, E., McDonald, C.P., Clow, D.W., & Striegl, R.G. (2016).
852 Aquatic carbon cycling in the conterminous United States and implications for terrestrial
853 carbon accounting. *Proceedings of the National Academy of Sciences*, 113(1), 58–63.
854 <https://doi.org/10.1073/pnas.1512651112>

855 Carey, C.C. & Breef-Pliz, A. (2022). Ice cover data for Falling Creek Reservoir, Vinton,
856 Virginia, USA for 2013-2022. (Version 4). [Dataset]. Environmental Data Initiative
857 (EDI). <https://portal.edirepository.org/nis/mapbrowse?packageid=edi.456.4>

858 Carey, C.C., Breef-Pilz, A. & Bookout, B.J. (2022c). Time series of high-frequency
859 meteorological data at Falling Creek Reservoir, Virginia, USA 2015-2021 (Version 14).
860 [Dataset]. Environmental Data Initiative (EDI). [https://portal-](https://portal-s.edirepository.org/nis/mapbrowse?scope=edi&identifier=143&revision=14)
861 [s.edirepository.org/nis/mapbrowse?scope=edi&identifier=143&revision=14](https://portal-s.edirepository.org/nis/mapbrowse?scope=edi&identifier=143&revision=14)

862 Carey, C.C., Breef-Pilz, A., Hounshell, A.G., Lofton, M.E., McClure, R.P., Gerling, A.B., &
863 Woelmer, W.M. (2022e). Discharge time series for the primary inflow tributary entering
864 Falling Creek Reservoir, Vinton, Virginia, USA 2013-2021. (Version 8). [Dataset].

865 Environmental Data Initiative (EDI).
866 <https://doi.org/10.6073/pasta/c65755d4c0102dde6e3140c1c91b77d6>

867 Carey, C.C., Breef-Pilz, A., Woelmer, W.M., & Bookout, B.J. (2022d). Time series of high-
868 frequency sensor data measuring water temperature, dissolved oxygen, pressure,
869 conductivity, specific conductance, total dissolved solids, chlorophyll a, phycocyanin,
870 and fluorescent dissolved organic matter at discrete depths in Falling Creek Reservoir,
871 Virginia, USA in 2018-2021. (Version 6). [Dataset]. Environmental Data Initiative (EDI).
872 <https://doi.org/10.6073/pasta/81c6c76f4fe22434a20aa8c00f2d4ad1>

873 Carey, C.C., Hounshell, A.G., D'Acunha, B.M., Breef-Pilz, A., Thomas, R.Q., & Johnson, M.S.
874 (2022a). Time series of carbon dioxide and methane fluxes measured with eddy
875 covariance for Falling Creek Reservoir in southwestern Virginia, USA during 2020-2022.
876 (Version 1). [Dataset]. Environmental Data Initiative (EDI).
877 <https://doi.org/10.6073/pasta/a1324bcf3e1415268996ba867c636489>

878 Carey, C.C., Hounshell, A.G., McClure, R.P., Gerling, A.B., Lewis, A.S.L., & Niederlehner,
879 B.R. (2022b). Time series of dissolved methane and carbon dioxide concentrations for
880 Falling Creek Reservoir and Beaverdam Reservoir in southwestern Virginia, USA during
881 2015-2021. (Version 6). [Dataset]. Environmental Data Initiative (EDI).
882 <https://doi.org/10.6073/pasta/2fb836492aace4c13b7962f2718be8e5>

883 Cole, J.J., & Caraco, N.F. (1998). Atmospheric exchange of carbon dioxide in a low-wind
884 oligotrophic lake measured by the addition of SF₆. *Limnology and Oceanography*, 43(4),
885 647–656. <https://doi.org/10.4319/lo.1998.43.4.0647>

886 Cole, J.J., Prairie, Y.T., Caraco, N.F., McDowell, W.H., Tranvik, L.J., Striegl, R.G., et. al.
887 (2007). Plumbing the Global Carbon Cycle: Integrating Inland Waters into the Terrestrial
888 Carbon Budget. *Ecosystems*, 10(1), 172–185. <https://doi.org/10.1007/s10021-006-9013-8>

889 Crusius, J., & Wanninkhof, R. (2003). Gas transfer velocities measured at low wind speed over a
890 lake. *Limnology and Oceanography*, 48(3), 1010–1017.
891 <https://doi.org/10.4319/lo.2003.48.3.1010>

892 D'Amario, S.C., & Xenopoulos, M.A. (2015). Linking dissolved carbon dioxide to dissolved
893 organic matter quality in streams. *Biogeochemistry*, 126(1–2), 99–114.
894 <https://doi.org/10.1007/s10533-015-0143-y>

895 Deemer, B.R., Harrison, J.A., Li, S., Beaulieu, J.J., DelSontro, T., Barros, et. al. (2016).
896 Greenhouse Gas Emissions from Reservoir Water Surfaces: A New Global Synthesis.
897 *BioScience*, 66(11), 949–964. <https://doi.org/10.1093/biosci/biw117>

898 Deemer, B.R., & Holgerson, M.A. (2021). Drivers of Methane Flux Differ Between Lakes and
899 Reservoirs, Complicating Global Upscaling Efforts. *Journal of Geophysical Research:*
900 *Biogeosciences*, 126(4). <https://doi.org/10.1029/2019JG005600>

901 DelSontro, T., del Giorgio, P.A., & Prairie, Y.T. (2018). No Longer a Paradox: The Interaction
902 Between Physical Transport and Biological Processes Explains the Spatial Distribution of
903 Surface Water Methane Within and Across Lakes. *Ecosystems*, 21(6), 1073–1087.
904 <https://doi.org/10.1007/s10021-017-0205-1>

905 Erkkilä, K.M., Ojala, A., Bastviken, D., Biermann, T., Heiskanen, J.J., Lindroth, A., et. al.
906 (2018). Methane and carbon dioxide fluxes over a lake: Comparison between eddy
907 covariance, floating chambers and boundary layer method. *Biogeosciences*, 15(2), 429–
908 445. <https://doi.org/10.5194/bg-15-429-2018>

909 Esters, L., Rutgersson, A., Nilsson, E., & Sahlée, E. (2021). Non-local Impacts on Eddy-
910 Covariance Air–Lake CO₂ Fluxes. *Boundary-Layer Meteorology*, 178(2), 283–300.
911 <https://doi.org/10.1007/s10546-020-00565-2>

912 Eugster, W. (2003). CO₂ exchange between air and water in an Arctic Alaskan and midlatitude
913 Swiss lake: Importance of convective mixing. *Journal of Geophysical Research*,
914 108(D12), 4362. <https://doi.org/10.1029/2002JD002653>

915 Eugster, W., DelSontro, T., & Sobek, S. (2011). Eddy covariance flux measurements confirm
916 extreme CH₄ emissions from a Swiss hydropower reservoir and
917 resolve their short-term variability. *Biogeosciences*, 8(9), 2815–2831.
918 <https://doi.org/10.5194/bg-8-2815-2011>

- 919 Gash, J.H.C., & Culf, A.D. (1996). Applying a linear detrend to eddy correlation data in
920 realtime. *Boundary Layer Meteorology*, 79, 301-306.
921 <https://doi.org/10.1007/BF00119443>
- 922 Gerling, A.B., Munger, Z.W., Doubek, J.P., Hamre, K.D., Gantzer, P.A., Little, J.C., & Carey,
923 C.C. (2016). Whole-Catchment Manipulations of Internal and External Loading Reveal
924 the Sensitivity of a Century-Old Reservoir to Hypoxia. *Ecosystems*, 19(3), 555–571.
925 <https://doi.org/10.1007/s10021-015-9951-0>
- 926 Golub, M., Desai, A.R., Vesala, T., Mammarella, I., Ojala, A., Bohrer, G., et. al. (2021). *New*
927 *insights into diel to interannual variation in carbon dioxide emissions from lakes and*
928 *reservoirs* [Preprint]. Environmental Sciences. <https://doi.org/10.1002/essoar.10507313.1>
- 929 Gómez-Gener, L., Rocher-Ros, G., Battin, T., Cohen, M.J., Dalmagro, H.J., Dinsmore, K.J., et.
930 al. (2021). Global carbon dioxide efflux from rivers enhanced by high nocturnal
931 emissions. *Nature Geoscience*, 14(5), 289–294. [https://doi.org/10.1038/s41561-021-](https://doi.org/10.1038/s41561-021-00722-3)
932 [00722-3](https://doi.org/10.1038/s41561-021-00722-3)
- 933 Gorsky, A.L., Lottig, N.R., Stoy, P.C., Desai, A.R., & Dugan, H.A. (2021). The Importance of
934 Spring Mixing in Evaluating Carbon Dioxide and Methane Flux From a Small North-
935 Temperate Lake in Wisconsin, United States. *Journal of Geophysical Research:*
936 *Biogeosciences*, 126(12). <https://doi.org/10.1029/2021JG006537>
- 937 Hanson, P.C., Pace, M.L., Carpenter, S.R., Cole, J.J., & Stanley, E.H. (2015). Integrating
938 Landscape Carbon Cycling: Research Needs for Resolving Organic Carbon Budgets of
939 Lakes. *Ecosystems*, 18(3), 363–375. <https://doi.org/10.1007/s10021-014-9826-9>
- 940 Heiskanen, J.J., Mammarella, I., Haapanala, S., Pumpanen, J., Vesala, T., MacIntyre, S., &
941 Ojala, A. (2014). Effects of cooling and internal wave motions on gas transfer
942 coefficients in a boreal lake. *Tellus B: Chemical and Physical Meteorology*, 66(1), 22827.
943 <https://doi.org/10.3402/tellusb.v66.22827>
- 944 Hounshell, A.G. (2022, July 11). aghounshell/EddyFlux: EddyFlux: Hounshell et al. 20XX re-
945 submission (Version 2.0.0). [Software] Zenodo. <https://doi.org/10.5281/zenodo.6818141>

946 Howard, D.W., Hounshell, A.G., Lofton, M.E., Woelmer, W.M., Hanson, P.C., & Carey, C.C.
947 (2021). Variability in fluorescent dissolved organic matter concentrations across diel to
948 seasonal time scales is driven by water temperature and meteorology in a eutrophic
949 reservoir. *Aquatic Sciences*, 83(2), 30. <https://doi.org/10.1007/s00027-021-00784-w>

950 Huotari, J., Ojala, A., Peltomaa, E., Nordbo, A., Launiainen, S., Pumpanen, J., et. al. (2011).
951 Long-term direct CO₂ flux measurements over a boreal lake: Five years of eddy
952 covariance data: CO₂ Fluxes of a boreal lake. *Geophysical Research Letters*, 38(18).
953 <https://doi.org/10.1029/2011GL048753>

954 Hyndman, R.J. & Athanasopoulos, G. (2018). *Forecasting: principles and practice*, 2nd Edition.
955 Otexts, Melbourne, Australia.

956 Hyndman, R., Athanasopoulos, G., Bergmeir, C., Caceres, G., Chhay, L., O'Hara-Wild, M., et al.
957 (2022, January 10). forecast: Forecasting functions for time series and linear models.
958 (Version 8.16). [Software]. R Package. <https://pkg.robjhyndman.com/forecast/>

959 Hyndman, R. J., & Khandakar, Y. (2008). Automatic Time Series Forecasting: The **forecast**
960 Package for R. *Journal of Statistical Software*, 27(3).
961 <https://doi.org/10.18637/jss.v027.i03>

962 Imrit, M.A., & Sharma, S. (2021). Climate Change is Contributing to Faster Rates of Lake Ice
963 Loss in Lakes Around the Northern Hemisphere. *Journal of Geophysical Research:*
964 *Biogeosciences*, 126(7). <https://doi.org/10.1029/2020JG006134>

965 Jammet, M., Crill, P., Dengel, S., & Friborg, T. (2015). Large methane emissions from a
966 subarctic lake during spring thaw: Mechanisms and landscape significance: Lake
967 methane emissions among spring thaw. *Journal of Geophysical Research:*
968 *Biogeosciences*, 120(11), 2289–2305. <https://doi.org/10.1002/2015JG003137>

969 Jammet, M., Dengel, S., Kettner, E., Parmentier, F.J.W., Wik, M., Crill, P., & Friborg, T. (2017).
970 Year-round CH₄ and CO₂ flux dynamics in two contrasting freshwater ecosystems of the
971 subarctic. *Biogeosciences*, 14(22), 5189–5216. <https://doi.org/10.5194/bg-14-5189-2017>

- 972 Jonsson, A., Åberg, J., Lindroth, A., & Jansson, M. (2008). Gas transfer rate and CO₂ flux
973 between an unproductive lake and the atmosphere in northern Sweden: CO₂ emission in
974 an unproductive lake. *Journal of Geophysical Research: Biogeosciences*, 113(G4).
975 <https://doi.org/10.1029/2008JG000688>
- 976 Klaus, M., Seekell, D.A., Lidberg, W., & Karlsson, J. (2019). Evaluations of Climate and Land
977 Management Effects on Lake Carbon Cycling Need to Account for Temporal Variability
978 in CO₂ Concentrations. *Global Biogeochemical Cycles*, 33(3), 243–265.
979 <https://doi.org/10.1029/2018GB005979>
- 980 Kljun, N., Calanca, P., Rotach, M.W., & Schmid, H.P. (2015). A simple two-dimensional
981 parameterisation for Flux Footprint Prediction (FFP). *Geoscientific Model Development*,
982 8(11), 3695–3713. <https://doi.org/10.5194/gmd-8-3695-2015>
- 983 Kljun, N., Rotach, M.W., & Schmid, H.P. (2002). A Three-Dimensional Backward Lagrangian
984 Footprint Model For A Wide Range Of Boundary-Layer Stratifications. *Boundary-Layer
985 Meteorology*, 103(2), 205–226. <https://doi.org/10.1023/A:1014556300021>
- 986 LiCor Biogeosciences. (2019, December 18). EddyPro® Software (Version 7.0.6) [Software].
987 LI-COR. <https://www.licor.com/env/support/EddyPro/home.html>
- 988 Liu, H., Zhang, Q., Katul, G.G., Cole, J.J., Chapin, F.S., & MacIntyre, S. (2016). Large CO₂
989 effluxes at night and during synoptic weather events significantly contribute to CO₂
990 emissions from a reservoir. *Environmental Research Letters*, 11(6), 064001.
991 <https://doi.org/10.1088/1748-9326/11/6/064001>
- 992 Lofton, M.E. (2022). melofton/FCR-phytos: Lofton et al. 20XX manuscript second revision
993 (Version 3.0.0.). [Software]. Zenodo. <https://doi.org/10.5281/zenodo.6483433>
- 994 Loken, L. C., Crawford, J.T., Schramm, P.J., Stadler, P., Desai, A.R., & Stanley, E.H. (2019).
995 Large Spatial and Temporal Variability of Carbon Dioxide and Methane in a Eutrophic
996 Lake. *Journal of Geophysical Research: Biogeosciences*, 124(7), 2248–2266.
997 <https://doi.org/10.1029/2019JG005186>

- 998 MacIntyre, S., Jonsson, A., Jansson, M., Aberg, J., Turney, D.E., & Miller, S.D. (2010).
999 Buoyancy flux, turbulence, and the gas transfer coefficient in a stratified lake.
1000 *Geophysical Research Letters*, 37(24). <https://doi.org/10.1029/2010GL044164>
- 1001 Mammarella, I., Nordbo, A., Rannik, Ü., Haapanala, S., Levula, J., Laakso, H., et. al. (2015).
1002 Carbon dioxide and energy fluxes over a small boreal lake in Southern Finland: CO₂ and
1003 Energy Fluxes Over Lake. *Journal of Geophysical Research: Biogeosciences*, 120(7),
1004 1296–1314. <https://doi.org/10.1002/2014JG002873>
- 1005 Mauder, M., & Foken T. (2006). Impact of post-field data processing on eddy covariance flux
1006 estimates and energy balance closure. *Meteorologische Zeitschrift*, 15, 597-609.
- 1007 McClure, R.P., Hamre, K.D., Niederlehner, B.R., Munger, Z.W., Chen, S., Lofton, M.E.,
1008 Schreiber, M.E., & Carey, C.C. (2018). Metalimnetic oxygen minima alter the vertical
1009 profiles of carbon dioxide and methane in a managed freshwater reservoir. *Science of The*
1010 *Total Environment*, 636, 610–620. <https://doi.org/10.1016/j.scitotenv.2018.04.255>
- 1011 McClure, R.P., Schreiber, M.E., Lofton, M.E., Chen, S., Krueger, K.M., & Carey, C.C. (2021).
1012 Ecosystem-Scale Oxygen Manipulations Alter Terminal Electron Acceptor Pathways in a
1013 Eutrophic Reservoir. *Ecosystems*, 24(6), 1281–1298. [https://doi.org/10.1007/s10021-020-](https://doi.org/10.1007/s10021-020-00582-9)
1014 [00582-9](https://doi.org/10.1007/s10021-020-00582-9)
- 1015 Moncrieff, J.B., Clement, R., Finnigan, J., Meyers, T. (2004). Averaging, Detrending, and
1016 Filtering of Eddy Covariance Time Series. In: Lee X., Massman W., Law B. (eds)
1017 *Handbook of Micrometeorology*. (Vol 29, pp. 7-31). Springer, Dordrecht.
1018 https://doi.org/10.1007/1-4020-2265-4_2
- 1019 Moncrieff, J.B., Massheder, J.M., de Bruin, H., Ebers, J., Friborg, T., Heusinkveld, B., et al.
1020 (1997). A system to measure surface fluxes of momentum, sensible heat, water vapor,
1021 and carbon dioxide. *Journal of Hydrology*, 188-189: 598-611.
1022 [https://doi.org/10.1016/S0022-1694\(96\)03194-0](https://doi.org/10.1016/S0022-1694(96)03194-0)
- 1023 Ouyang, Z., Shao, C., Chu, H., Becker, R., Bridgeman, T., Stepien, C., John, R., & Chen, J.
1024 (2017). The Effect of Algal Blooms on Carbon Emissions in Western Lake Erie: An

1025 Integration of Remote Sensing and Eddy Covariance Measurements. *Remote Sensing*,
1026 9(1), 44. <https://doi.org/10.3390/rs9010044>

1027 Podgrajsek, E., Sahlée, E., Bastviken, D., Holst, J., Lindroth, A., Tranvik, L., & Rutgersson, A.
1028 (2014). Comparison of floating chamber and eddy covariance measurements of lake
1029 greenhouse gas fluxes. *Biogeosciences*, 11(15), 4225–4233. [https://doi.org/10.5194/bg-](https://doi.org/10.5194/bg-11-4225-2014)
1030 [11-4225-2014](https://doi.org/10.5194/bg-11-4225-2014)

1031 Podgrajsek, E., Sahlée, E., Bastviken, D., Natchimuthu, S., Kljun, N., Chmiel, H.E.,
1032 Klemedtsson, L., & Rutgersson, A. (2016). Methane fluxes from a small boreal lake
1033 measured with the eddy covariance method: Methane fluxes from a small boreal lake.
1034 *Limnology and Oceanography*, 61(S1), S41–S50. <https://doi.org/10.1002/lno.10245>

1035 Prairie, Y.T., Alm, J., Beaulieu, J., Barros, N., Battin, T., Cole, J., et. al. (2018). Greenhouse Gas
1036 Emissions from Freshwater Reservoirs: What Does the Atmosphere See? *Ecosystems*,
1037 21(5), 1058–1071. <https://doi.org/10.1007/s10021-017-0198-9>

1038 Read, J.S., Hamilton, D.P., Desai, A.R., Rose, K.C., MacIntyre, S., Lenters, J.D., et al. (2012).
1039 Lake-size dependency of wind shear and convection as controls on gas exchange: lake-
1040 size dependency of u^* and w^* . *Geophysical Research Letters*, 39(9).
1041 <https://doi.org/10.1029/2012GL051886>

1042 Reed, D.E., Dugan, H.A., Flannery, A.L., & Desai, A.R. (2018). Carbon sink and source
1043 dynamics of a eutrophic deep lake using multiple flux observations over multiple years.
1044 *Limnology and Oceanography Letters*, 3(3), 285–292. <https://doi.org/10.1002/lol2.10075>

1045 Rosentreter, J.A., Borges, A.V., Deemer, B.R., Holgerson, M.A., Liu, S., Song, C., et al. (2021).
1046 Half of global methane emissions come from highly variable aquatic ecosystem sources.
1047 *Nature Geoscience*, 14(4), 225–230. <https://doi.org/10.1038/s41561-021-00715-2>

1048 Sanches, L.F., Guenet, B., Marinho, C.C., Barros, N., & de Assis Esteves, F. (2019). Global
1049 regulation of methane emission from natural lakes. *Scientific Reports*, 9(1), 255.
1050 <https://doi.org/10.1038/s41598-018-36519-5>

- 1051 Scholz, K., Ejarque, E., Hammerle, A., Kainz, M., Schelker, J., & Wohlfahrt, G. (2021).
1052 Atmospheric CO₂ Exchange of a Small Mountain Lake: Limitations of Eddy Covariance
1053 and Boundary Layer Modeling Methods in Complex Terrain. *Journal of Geophysical*
1054 *Research: Biogeosciences*, 126(7). <https://doi.org/10.1029/2021JG006286>
- 1055 Shao, C., Chen, J., Stepien, C.A., Chu, H., Ouyang, Z., Bridgeman, T.B., Czajkowski, K.P.,
1056 Becker, R.H., & John, R. (2015). Diurnal to annual changes in latent, sensible heat, and
1057 CO₂ fluxes over a Laurentian Great Lake: A case study in Western Lake Erie. *Journal of*
1058 *Geophysical Research: Biogeosciences*, 120(8), 1587–1604.
1059 <https://doi.org/10.1002/2015JG003025>
- 1060 Sharma, S., Richardson, D.C., Woolway, R.I., Imrit, M.A., Bouffard, D., Blagrove, K., et. al.
1061 (2021). Loss of Ice Cover, Shifting Phenology, and More Extreme Events in Northern
1062 Hemisphere Lakes. *Journal of Geophysical Research: Biogeosciences*, 126(10).
1063 <https://doi.org/10.1029/2021JG006348>
- 1064 Siczko, A. K., Duc, N.T., Schenk, J., Pajala, G., Rudberg, D., Sawakuchi, H.O., & Bastviken,
1065 D. (2020). Diel variability of methane emissions from lakes. *Proceedings of the National*
1066 *Academy of Sciences*, 117(35), 21488–21494. <https://doi.org/10.1073/pnas.2006024117>
- 1067 Smith, S.V., Renwick, W.H., Bartley, J.D., & Buddemeier, R.W. (2002). Distribution and
1068 significance of small, artificial water bodies across the United States landscape. *Science*
1069 *of The Total Environment*, 299(1–3), 21–36. [https://doi.org/10.1016/S0048-](https://doi.org/10.1016/S0048-9697(02)00222-X)
1070 [9697\(02\)00222-X](https://doi.org/10.1016/S0048-9697(02)00222-X)
- 1071 Sobek, S., Tranvik, L.J., & Cole, J.J. (2005). Temperature independence of carbon dioxide
1072 supersaturation in global lakes: Carbon dioxide supersaturation in global lakes. *Global*
1073 *Biogeochemical Cycles*, 19(2),. <https://doi.org/10.1029/2004GB002264>
- 1074 Soloviev, A., Donelan, M., Graber, H., Haus, B., & Schlüssel, P. (2007). An approach to
1075 estimation of near-surface turbulence and CO₂ transfer velocity from remote sensing
1076 data. *Journal of Marine Systems*, 66(1–4), 182–194.
1077 <https://doi.org/10.1016/j.jmarsys.2006.03.023>

1078 Taoka, T., Iwata, H., Hirata, R., Takahashi, Y., Miyabara, Y., & Itoh, M. (2020). Environmental
1079 Controls of Diffusive and Ebullitive Methane Emissions at a Subdaily Time Scale in the
1080 Littoral Zone of a Midlatitude Shallow Lake. *Journal of Geophysical Research:*
1081 *Biogeosciences*, 125(9). <https://doi.org/10.1029/2020JG005753>

1082 Tranvik, L.J., Downing, J.A., Cotner, J.B., Loiselle, S.A., Striegl, R.G., Ballatore, T.J., et. al.
1083 (2009). Lakes and reservoirs as regulators of carbon cycling and climate. *Limnology and*
1084 *Oceanography*, 54(6part2), 2298–2314. https://doi.org/10.4319/lo.2009.54.6_part_2.2298

1085 USACE (United States Army Corps of Engineers). (2021). National inventory of Dams (NID).
1086 [accessed 2022 February 7]. <https://nid.usace.army.mil/#/>

1087 Vachon, D., & Prairie, Y.T. (2013). The ecosystem size and shape dependence of gas transfer
1088 velocity versus wind speed relationships in lakes. *Canadian Journal of Fisheries and*
1089 *Aquatic Sciences*, 70(12), 1757–1764. <https://doi.org/10.1139/cjfas-2013-0241>

1090 Vesala, T., Eugster, W., & Ojala, A. (2012). Eddy Covariance Measurements over Lakes. In M.
1091 Aubinet, T. Vesala, & D. Papale (Eds.), *Eddy Covariance* (pp. 365–376). Springer
1092 Netherlands. https://doi.org/10.1007/978-94-007-2351-1_15

1093 Vesala, T., Huotari, J., Rannik, Ü., Suni, T., Smolander, S., Sogachev, A., Launiainen, S., &
1094 Ojala, A. (2006). Eddy covariance measurements of carbon exchange and latent and
1095 sensible heat fluxes over a boreal lake for a full open-water period. *Journal of*
1096 *Geophysical Research*, 111(D11), D11101. <https://doi.org/10.1029/2005JD006365>

1097 Vickers, D., & Mahrt, L. (1997). Quality Control and Flux Sampling Problems for Tower and
1098 Aircraft Data. *Journal of Atmospheric and Oceanic Technology*, 14(3), 512–526.
1099 [https://doi.org/10.1175/1520-0426\(1997\)014<0512:QCAFSP>2.0.CO;2](https://doi.org/10.1175/1520-0426(1997)014<0512:QCAFSP>2.0.CO;2)

1100 Waldo, S., Beaulieu, J.J., Barnett, W., Balz, D. A., Vanni, M.J., Williamson, T., & Walker, J.T.
1101 (2021). Temporal trends in methane emissions from a small eutrophic reservoir: The key
1102 role of a spring burst. *Biogeosciences*, 18(19), 5291–5311. [https://doi.org/10.5194/bg-18-](https://doi.org/10.5194/bg-18-5291-2021)
1103 [5291-2021](https://doi.org/10.5194/bg-18-5291-2021)

- 1104 Watras, C.J., Morrison, K.A., Crawford, J.T., McDonald, C.P., Oliver, S.K., & Hanson, P.C.
1105 (2015). Diel cycles in the fluorescence of dissolved organic matter in dystrophic
1106 Wisconsin seepage lakes: Implications for carbon turnover: Diel CDOM fluorescence
1107 cycles. *Limnology and Oceanography*, 60(2), 482–496. <https://doi.org/10.1002/lno.10026>
- 1108 Webb, E.K., Pearman, G.I., & Leuning R. (1980). Correction of flux measurements for density
1109 effects due to heat and water vapour transfer. *Quarterly Journal of the Royal*
1110 *Meteorological Society*, 106(447), 85-100. <https://doi.org/10.1002/qj.49710644707>
- 1111 Wik, M., Thornton, B.F., Bastviken, D., Uhlbäck, J., & Crill, P.M. (2016). Biased sampling of
1112 methane release from northern lakes: A problem for extrapolation. *Geophysical Research*
1113 *Letters*, 43(3), 1256–1262. <https://doi.org/10.1002/2015GL066501>
- 1114 Wilczak, J.M., Oncley, S.P., Stage, S.A. (2001). Sonic anemometer tilt correction algorithms.
1115 *Boundary-Layer Meteorology*, 99, 127-150. <https://doi.org/10.1023/A:1018966204465>
- 1116 Winslow, L. A., Read, J.S., Hanson, P.C., & Stanley, E.H. (2014). Lake shoreline in the
1117 contiguous United States: Quantity, distribution and sensitivity to observation resolution.
1118 *Freshwater Biology*, 59(2), 213–223. <https://doi.org/10.1111/fwb.12258>
- 1119 Winslow, L., Read, J., Woolway, R., Brentrop, J., Leach T., Zwart, J., Albers, S., & Collinge, C.
1120 (2016a, June 9). LakeAnalyzer: Lake Physics Tools. (Version 1.11.4.1). [Software]. R.
1121 Package. <https://CRAN.R-project.org/package=rLakeAnalyzer>
- 1122 Winslow, L.A., Zwart, J.A., Batt, R.D., Dugan, H.A., Woolway, R.I., Corman, J.R., Hanson,
1123 P.C., & Read, J.S. (2016c). LakeMetabolizer: An R package for estimating lake
1124 metabolism from free-water oxygen using diverse statistical models. *Inland Waters*, 6(4),
1125 622–636. <https://doi.org/10.1080/IW-6.4.883>
- 1126 Winslow, L., Zwart, J., Batt, R., Corman, J., Dugan, H., Hanson, P., et. al. (2016b, June 23).
1127 LakeMetabolizer: Tools for the analysis of ecosystem metabolism. (Version 1.5.0).
1128 [Software]. R Package. <https://CRAN.R-project.org/pacakge=LakeMetabolizer>

- 1129 Woolway, R.I., Kraemer, B.M., Lenters, J.D., Merchant, C.J., O'Reilly, C.M., & Sharma, S.
1130 (2020). Global lake responses to climate change. *Nature Reviews Earth & Environment*,
1131 *1*(8), 388–403. <https://doi.org/10.1038/s43017-020-0067-5>
- 1132 Wutzler, T., Lucas-Moffat, A., Migliavacca, M., Knauer, J., Sickel, K., Šigut, L., Menzer, O., &
1133 Reichstein, M. (2018). Basic and extensible post-processing of eddy covariance flux data
1134 with REddyProc. *Biogeosciences*, *15*(16), 5015–5030. [https://doi.org/10.5194/bg-15-](https://doi.org/10.5194/bg-15-5015-2018)
1135 [5015-2018](https://doi.org/10.5194/bg-15-5015-2018)
- 1136 Wutzler, T., Reichstein, M., Lucas-Moffat, A.M., Menzer, O., Migliavacca, M., & Sickel, K.
1137 (2021, December 01). REddyProc: Post Processing of (Half-) Hourly Eddy-Covariance
1138 Measurements. (Version 1.3.1). [Software]. R. Package. [https://CRAN.R-](https://CRAN.R-project.org/package=REddyProc)
1139 [project.org/package=REddyProc](https://CRAN.R-project.org/package=REddyProc)